Czech Technical University in Prague
Faculty of Electrical Engineering
Department of Electromagnetic Field

Measurement of multi–antenna communication channels – study of upper bound channel capacity based on eigenvalue decomposition

Master's Thesis

Bc. Tomáš Janák

Master's programme: Electronics and Communication
Branch of study: Radio and Optical Technology
Supervisor: Ing. Rostislav Karásek

Prague, May 2019

Declaration

I hereby declare I have written this paper independently and quoted all the sources of information used in accordance with methodological instructions on ethical principles for writing an academic thesis. Moreover, I state that this thesis has neither been submitted nor accepted for any other degree.

In Prague, May 2019

.....
Bc. Tomáš Janák

ZADÁNÍ DIPLOMOVÉ PRÁCE

I. OSOBNÍ A STUDIJNÍ ÚDAJE

Příjmení: **Janák** Jméno: **Tomáš** Osobní číslo: **406507**

Fakulta/ústav: **Fakulta elektrotechnická**

Zadávající katedra/ústav: **Katedra elektromagnetického pole**

Studijní program: **Elektronika a komunikace**

Studijní obor: **Rádiová a optická technika**

II. ÚDAJE K DIPLOMOVÉ PRÁCI

Název diplomové práce:

Measurement of multi-antenna communication channels - study of upper bound channel capacity based on eigenvalue decomposition

Název diplomové práce anglicky:

Measurement of multi-antenna communication channels - study of upper bound channel capacity based on eigenvalue decomposition

Pokyny pro vypracování:

- Study prior work including the theory of a multi-antenna communication and methods of measurement of such wireless communication technique.
- Investigate how is the eigenvalue decomposition used for wireless communication coding.
- Based on the state-of-the-art of multiantenna solution measurement, implement a simplified non-line-of-sight multiantenna scenario using simulation technique. Then recreate this scenario in an anechoic chamber and compare the results of your simulation and experiment with the theory.
- Based on the gathered knowledge, suggest a suitable measurement method for future generation of wireless communication, e.g., 5th Generation of cellular mobile communication.
- Perform measurement of your proposed multiantenna solution in an selected indoor scenario, process the measurement data and interpret them. Compare your results with the theory and state-of-the-art measurement techniques.

Consultant Specialist: Prof Ing. Pavel Pechač, Ph.D.

Seznam doporučené literatury:

[1] B. Vucetic and J. Yuan, Space-time coding, Wiley, 2003.
[2] H. Jafarkhani, Space-time coding theory and practice, Cambridge University Press, 2005.
[3] G.J. Foschini and M.J. Gans, “On limits of wireless communications in a fading environment when using multiple antennas,” Wireless Personal Communications, vol. 6, 1998, pp. 311–335.
[4] T. L. Marzetta and J. Salz, "Singular value decomposition of a matrix-valued impulse response," Proceedings. (ICASSP '05). IEEE International Conference on Acoustics, Speech, and Signal Processing, 2005., Philadelphia, PA, 2005, pp. iv/913-iv/916 Vol. 4. doi: 10.1109/ICASSP.2005.1416158
[5] P. L. Kafle, A. Intarapanich, A. B. Sesay, J. Mcrory and R. J. Davies, "Spatial correlation and capacity measurements for wideband MIMO channels in indoor office environment," in IEEE Transactions on Wireless Communications, vol. 7, no. 5, pp. 1560-1571, May 2008. doi: 10.1109/TWC.2008.060170

Acknowledgements

I would like to acknowledge and thank the following important people who have supported me, not only during the course of this thesis but throughout all my Master's degree. Firstly, I would like to express my gratitude to my supervisor Ing. Rostislav Karásek, for his great support and all the advice. I would also like to thank Ing. Pavel Pechač Ph.D. for providing me with all the necessary guidance and insight throughout the research. Special thanks go to Ing. Václav Kabourek for unwavering support during the measurement. Moreover, finally, I would like to thank my family and close friends. You have all encouraged me and supported me.

Abstract

The content of the work is a study on quality of the wireless communication inside a building with stress put on the multi–antenna systems. The thesis contains a theoretical basis of the propagation of the electromagnetic waves in such Multiple–Input Multiple–Output (MIMO) channel, taking into the account only relevant properties of such propagation. The emphasis is put on the diversity and gain of the systems and capacity of the MIMO channel. A linear algebra numerical tool called Singular Value Decomposition (SVD) is used to calculate channel capacity. The simulation part utilizes SVD to determine a capacity of the defined scenario and then the results are compared to the measurement in the anechoic chamber. The practical part consists of the measurement in the real scenario and calculating of the channel capacity using same tools as in the simulation part. At the end, the results are discussed with regards to possible practical use of those results.

Abstrakt

Tématem této práce je posouzení kvality bezdrátového přenosu uvnitř budovy, zejména s ohledem na využití multianténních systémů. Obsahem práce jsou teoretické základy bezdrátové komunikace pro Multiple–Input Multiple–Output (MIMO) kanály, kdy jsou brány v úvahu pouze takové vlastnosti šíření spjaté s tímto druhem šíření elektromagnetických vln. Důraz je kladen na diverzitu a zisk MIMO systémů a kapacitu jím odpovídajících MIMO kanálů. V simulační části práce se využívá Singular Value Decomposition (SVD), jakožto numerický výpočetní nástroj lineární algebry často využívaný k výpočtu kapacity kanálu, k určení kapacity v definovaném scénáři a poté jsou tyto výsledky ověřeny měřením v bezodrazové komoře. Praktická část se skládá z měření v reálném scénáři a výpočtu kapacity kanálu pomocí stejné metody jako v simulační části. Na závěr jsou diskutovány výsledky získané měřením a simulací, s ohledem na případné využití těchto výsledků v praxi.

Keywords

MIMO channel, singular value decomposition, capacity, diversity, gain, flat–frequency channel, transfer function, eigenvalues, eigenvectors

Klíčová slova

MIMO kanál, singulární rozklad matice, kapacita, diversita, zisk, frekvenčně plochý kanál, přenosová funkce, singulární čísla, singulární vektory

List of Tables

List of Figures

List of Acronyms

CDF Cumulative Distribution Function.

CSI Channel State Information.

FSL Free Space Loss.

IID Independent Identically Distributed.

LOS Line–Of–Sight.

MIMO Multiple–Input Multiple–Output.

MISO Multiple–Input Multiple–Output.

MPC MultiPath Component.

MRC Maximum Ration Combining.

NLOS Non–Line–Of–Sight.

PDP Power Delay Profile.

RMS Root Mean Square.

SIMO Single–Input Multiple–Output.

SISO Single–Input Single–Output.

SMG Spatial Multiplexing Gain.

SNR Signal to Noise Ratio.

SVD Singular Value Decomposition.

VNA Vector Network Analyzer.

Contents

Chapter 1

Introduction

Multiple–Input Multiple–Output (MIMO) systems have had the key role in wireless communications for years already. Many standards including WiFi, mobile systems of the 3rd and the 4th generation uses MIMO as an essential tool for enhancing capacity, transmission rates, and reliability of the wireless networks.

Reliability and capacity related to higher transmission rates can be improved using diversity and spatial multiplexing in MIMO systems without increasing the transmitted power. Diversity is a mean to provide multiple different forms of the transmitted signal with various independent fading useful at the receiving (RX) antenna for better decoding of the received signal. While the diversity is linked with the RX antennas, spatial multiplexing, on the other hand, is linked with the transmitting (TX) antennas. It allows transmitting a parallel stream of symbols from the transmitter. Both these phenomena are used in MIMO systems simultaneously, but they cannot be optimized at once.

The thesis contains some basics from the theory of the wireless communications related to the MIMO channel, especially the difference between flat–fading and selective–fading channel. Several types of gains are discussed in this part, as well as the theory regarding MIMO channel itself (channel matrix, closed vs. open loop systems). The main goal of the work is the calculation of the channel capacity utilizing eigenvalue decomposition of the channel matrix.

The Singular Value Decomposition (SVD) is a computational tool in the linear algebra commonly used to estimate the matrix rank, solve linear least squares problems and last but not least, is to tell for any matrix $\mathbf{A}$ its orthogonal matrices $\mathbf{U}$ and $\mathbf{V}$ and a diagonal matrix $\mathbf{S}$ such that $\mathbf{A} = \mathbf{USV}^{\mathrm{H}}$, where H is a conjugate transpose. These matrices of eigenvectors and eigenvalues are used for the data precoding on the transmitter side to send the data over orthogonal paths and on the receiver side to proper separation of these paths. The practical part contains a simplified simulation of the 2×2 MIMO scenario. The capacity results and radiation patterns are presented and verified by the measurement

of the same scenario in the anechoic chamber. The last part of the thesis is focused on the measurement and capacity estimation of the channel in a real indoor scenario.

Chapter 2

Wireless Communication

2.1 Fading

Wireless channels can be uniquely described as the channels with different paths between transmitting and receiving antennas. Then, fading is caused by interference of multiple versions of the transmitted signal within these paths. These multipath signals are combined at the receiver and create the resulting signal. This signal can change its strength rapidly and is random. Thus, we call such a channel time–varying fading channel, and is shown in Fig. 2.1. In such a model, we are describing changes of a length of the individual paths between transmitter and receiver antennas as a change of a propagation delay of the individual signal replicas, and is described with linear time–varying impulse response $h(t, \tau)$.

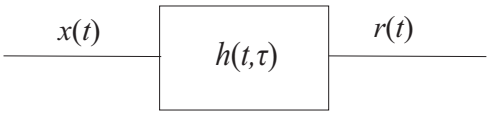

Figure 2.1: Time–varying channel model with impulse response.

The channel with the constant gain and linear phase response over a greater bandwidth than the bandwidth of the transmitted signal is called a flat–fading channel. It means that in the frequency domain, all components are delayed by the same time value, which equals to the slope of the linear function. The channel impulse response of such a channel can be expressed by a single delta function:

$$h(t, \tau) = \alpha(t)\,\delta(\tau), \tag{2.1}$$

where $\delta(t)$ is the Dirac delta function and α is a time–varying amplitude. If the actual channel impulse response can be expressed as in (2.1), then the transit of the signal $x(t)$ through the channel can be expressed as a convolution (product of two functions as one

is reversed and shifted) of the signal and the impulse response as illustrated in Fig. 2.2.

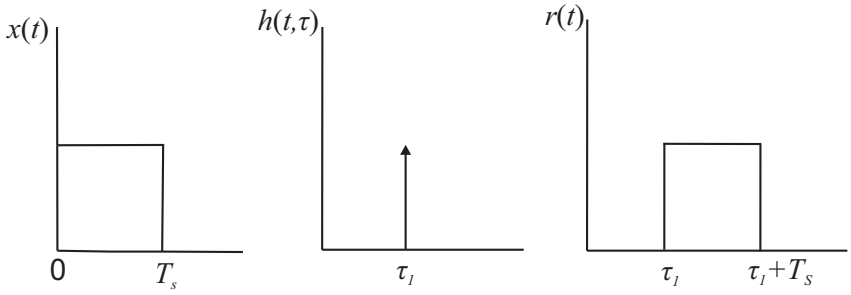

Figure 2.2: Influence of the flat fading channel on the signal.

The convolution, denoted by asterisk, can be expressed as follows:

$$r\left(t\right) = x\left(t\right) * h\left(t\right) = \int_{-\infty}^{\infty} x\left(\tau\right) h\left(t-\tau\right) \mathrm{d}\tau. \tag{2.2}$$

The channel coherence bandwidth B_c is defined for fading channels as statistical property of the channel. It applies that the channel is considered to be flat in this frequency range. The coherence bandwidth is derived using delay spread. Delay spread is defined using I paths in the multipath channel, power p_i of the i^{th} path and delay τ_i of the i^{th}.

Then, the probability–weighted average value of the delay is given by [1] :

$$\overline{\tau} = \frac{\sum_{i=1}^{I} p_i \tau_i}{\sum_{i=1}^{I} p_i}. \tag{2.3}$$

The variance of a delay is then given by [1] :

$$\sigma_t = \sqrt{\overline{\tau^2} - \overline{\tau}^2}, \tag{2.4}$$

where $\overline{\tau^2}$ denotes [1]:

$$\overline{\tau^2} = \frac{\sum_{i=1}^{I} p_i \tau_i^2}{\sum_{i=1}^{I} p_i}. \tag{2.5}$$

Finally, the coherence bandwidth of the channel is:

$$B_c = \frac{1}{5\sigma_t}, \tag{2.6}$$

using confidence interval 2.5σ (confidence of 98.76%). For the flat fading channel applies that $B_c > B_s$ where B_s is the bandwidth of the signal going through the channel.

On the other hand, in the frequency selective fading channel, each frequency component can suffer from a different delay in the time domain. The impulse response of such a channel is shown in Fig. 2.3 and can be expressed as a series of delta functions as follows [1]:

$$h(t,\tau) = \sum_{j=1}^{J} \alpha_j(t)\delta(\tau - \tau_j), \tag{2.7}$$

where $\alpha_j(t)$ is independent of $\alpha_i(t)$ for $j \neq i$.

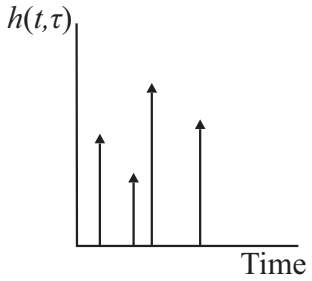

Figure 2.3: Impulse response of the frequency selective fading channel [1].

In such channel the coherence bandwidth is smaller than the bandwidth of the signal going through the channel. Thus, we have to investigate properties of the channel, especially impulse response. The frequency selective fading in the channel is illustrated in Fig. 2.4. Let us assume channel impulse response as there are two identical delta functions shifted by $\tau_2 - \tau_1$ from each other. We can observe that the gain varies in time. The variations in gain are present because of the small enough time difference between delta functions in the impulse response. If the time difference was larger, two pulses at the output would be present.

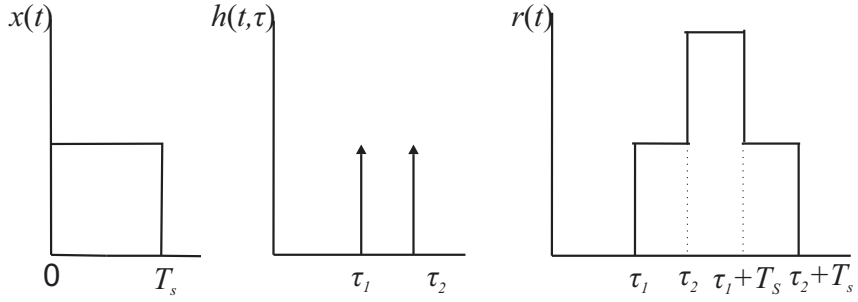

Figure 2.4: Influence of the frequency selective fading channel on the signal.

2.2 Diversity

Fading can cause a significant decrease of the received power at the receiver. The fading is caused by the destructive interference of the multipath components or interference from other users. As the thermal noise at the receiver is rather "stable", Signal to Noise Ratio (SNR) at the receiver is changing according to the fading. The receiver itself needs a minimum SNR for reliable functionality so the transmitted signal can be detected and decoded successfully. If the SNR is below the minimum value, the transmitted signal is not recovered, and there is an outage.

Diversity of a signal on the receiver can be used to decrease the probability of error. The symbol error probability P_{e} is a wrong detection of data symbol on the receiver side after passing through the channel. Diversity means that there are different versions of the same transmitted signal at the receiver where they can be combined. To provide various versions of the transmitted signal to the receiver without the need of increasing transmission power, it needs to be ensured the data symbols pass through multiple signal paths. Thus, these different versions of the signal have independent fading and the outage probability. A probability that the receiver cannot reliably detect and decode the transmitted signal is much smaller than in the channel without diversity. In such channel we define the diversity gain as [1]:

$$G_{\mathrm{d}} = -\lim_{\rho\to\infty} \frac{\log\left(P_{\mathrm{e}}\right)}{\log\left(\rho\right)}, \tag{2.8}$$

where P_{e} is the error probability. There are many ways how to obtain diversity:

- time–temporal diversity
- frequency–frequency diversity
- polarization–spatial diversity
- antenna–antenna diversity.

Then we have to deal with the processing at the receiver. We use various combining methods to reach this goal and to reduce the probability of error at the receiver. There are two important combining methods:

- Maximum Ration Combining (MRC)
- Selection Combining.

More on these combining methods can be found in [1].

2.3 Spatial Multiplexing

While diversity gain is obtained by using multiple receiving antennas, spatial multiplexing, on the other hand, uses multiple transmitting antennas. Thus, a serial stream of the symbols is converted to the parallel stream transmitted simultaneously from the transmitting antennas. We use spatial multiplexing to achieve higher transmission rates; the rate relates to channel capacity, which can be increased in MIMO systems by raising the SNR. Thus, we can define Spatial Multiplexing Gain (SMG), denoted as G_{SMG}, as follows [1]:

$$G_{\mathrm{SMG}} = \lim_{\rho \to \infty} \frac{r}{\log(\rho)}, \tag{2.9}$$

where r is the code rate at the transmitter in bits/channel as a function of the SNR. Spatial multiplexing gain is related to the rate similarly as diversity gain is related to the probability of error.

2.4 Trade–Off Between Spatial Multiplexing and Diversity

Diversity and spatial multiplexing in the channel achieved by both transmitting and receiving antennas are used within MIMO systems. Especially if multiple transmitters are used, we can achieve not only high diversity but other advantages as well, such as higher channel capacity and transmission rate. Assume MIMO channel where the number of transmitting antennas N_{t} and number of the receiving antennas N_{r} is the same, then according to [1] channel capacity can linearly increase with the number of antennas, and there is no need to increase transmission power. Furthermore, for a different number of receivers and transmitters system is able to transmit $\min(N_{\mathrm{t}}, N_{\mathrm{r}})$ symbols per time slot. If $N_{\mathrm{t}} < N_{\mathrm{r}}$ symbols can be transmitted with the diversity gain $N_{\mathrm{t}} - N_{\mathrm{r}} + 1$. Note, that for the same number of antennas mentioned above, diversity gain equals one. The channel capacity per unit channel bandwidth can be given as [2]:

$$C \approx \min(N_{\mathrm{t}}, N_{\mathrm{r}}) \log_2(1 + \rho). \tag{2.10}$$

However, both diversity gain and multiplexing gain cannot be optimized at once. When we optimize first, we have to trade–off second and vice versa. There is a formula defining the trade–off between diversity and multiplexing [2]:

$$G_{\mathrm{dopt}} = (N_{\mathrm{t}} - G_{\mathrm{SMG}})(N_{\mathrm{r}} - G_{\mathrm{SMG}}), \tag{2.11}$$

where G_{dopt} is optimal diversity gain for given multiplexing gain G_{SMG}.

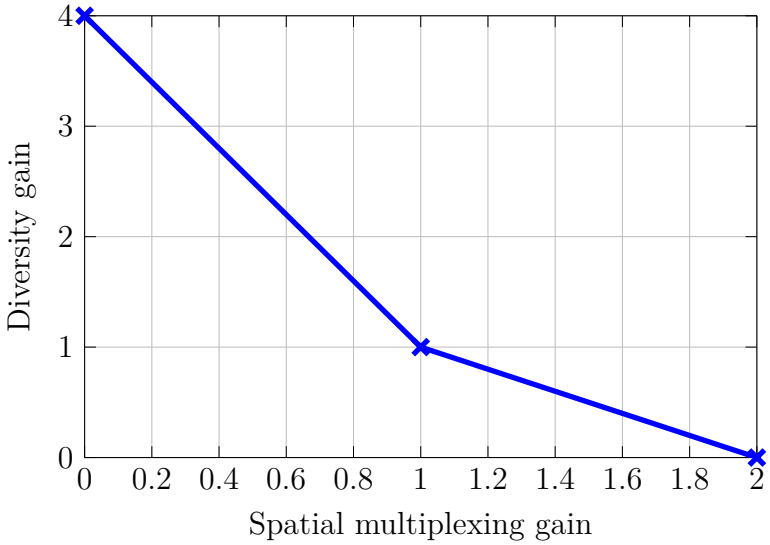

Figure 2.5: Optimal trade–off for 2×2 MIMO.

The (2.11) expresses a dual behavior of the MIMO channel; multiplexing gain is obtained for non–interfering parallel links between antennas and, at the same time, diversity is obtained, assuming that link from the transmitting antenna is available to every receiving antenna. An example of the optimal trade–off for 2×2 MIMO channel is shown in Fig. 2.5:

2.5 MIMO Channels

Electromagnetic waves propagate through wireless channels in many ways, especially in a rich scattering environment. Electromagnetic wave undergoes mainly reflection, scattering, diffraction, and refraction. These physical processes cause a change of the magnitude and phase of all multipath components in the channel. The magnitude and phase of these components can be expressed as the complex number, and so the received signal can be expressed simply as the sum of the components. The real and imaginary components are Gaussian distributed random variables. In case, the multipath components have uniform phase and all have similar amplitude, the envelope of their sum follows Rayleigh distribution since the mean value of real and imaginary part is zero. However, if there is one significant multipath stronger than the others, the envelope of their sum follows Ricean distribution. Assume N_{t} transmitting antennas and N_{r} receiving antennas in a MIMO system ($N_{\mathrm{t}}\times N_{\mathrm{r}}$ MIMO). In such system, there are $N_{\mathrm{t}}N_{\mathrm{r}}$ paths between transmitter and receiver.

Thus, the channel can be represented as a matrix with $N_\mathrm{r} \times N_\mathrm{t}$ elements, and the received signal can be expressed as [2]:

$$\mathbf{r} = \mathbf{H}\mathbf{x} + \mathbf{n}. \tag{2.12}$$

Matrix $\mathbf{H}$ with dimensions $N_\mathrm{r} \times N_\mathrm{t}$ is called channel matrix. Matrix of transmitted signals $\mathbf{x}$ is a matrix of dimension $N_\mathrm{t} \times \mathrm{T}$ and $\mathbf{n}$ is noise matrix with the same dimensions as $\mathbf{r}$, where T is number of transmitting time slots, for 1 time slot the matrix equation is given by [2]:

$$\begin{bmatrix} r_1 \\ r_2 \\ \vdots \\ r_{N_\mathrm{r}} \end{bmatrix} = \begin{bmatrix} h_{11} & h_{12} & \dots & h_{1N_\mathrm{t}} \\ h_{21} & h_{22} & \dots & h_{2N_\mathrm{t}} \\ \vdots & \vdots & \ddots & \vdots \\ h_{N_\mathrm{r}1} & h_{N_\mathrm{r}1} & \dots & h_{N_\mathrm{r}N_\mathrm{t}} \end{bmatrix} \begin{bmatrix} x_1 \\ x_2 \\ \vdots \\ x_{N_\mathrm{t}} \end{bmatrix} + \begin{bmatrix} n_1 \\ n_2 \\ \vdots \\ n_{N_\mathrm{r}} \end{bmatrix},$$

where r_i is the signal received by i^{th} antenna, x_j is the symbol transmitted by the j^{th} antenna and h_{ij} is the complex channel coefficient of the path between i^{th} and j^{th} antenna. We assume independent channel path gains, noise samples, and transmitted symbols are independent of each other. This assumption is valid for the spatial domain, and distance at least half of the wavelength l between two chosen antennas [1]. Thus, h_{ij} is independent of $h_{i'j'}$ for $i \neq i'$ or $j \neq j'$. If this condition is not met, some spatial correlation exists, and channel coefficients are not independent. Furthermore, channel gains are not independent. We also assume noise as zero–mean circularly symmetric complex Gaussian random variable, and bandwidth to be narrow enough, so the channel is flat over a frequency band [1]. In other words, we defined such channel as a frequency non–selective, and the channel matrix is constant over the given frequency band.

We can differ two kinds of MIMO systems based on the amount of information about the channel at the transmitter and receiver:

- Open–loop system is such a system, where the transmitter has no information about the channel at all. There is no feedback between the transmitter and the receiver about the state of the channel. The receiver is able to learn the channel state from some training sequence and provide Channel State Information (CSI) though. This kind of system can be easily obtained, as there is no need for feedback or calibration.

- Closed–loop system differs from the previous one; there is knowledge about the channel at the transmitter. The CSI obtained at the receiver is sent to the transmitter, where it can be used to adjust the transmission to achieve better performance. Nevertheless, CSI at the transmitter is hard to obtain as "we have to make sure that feedback occurs within a time that is less than the coherence time of the channel"[3]. At the same time, the feedback decreases the spectral efficiency of the channel as CSI carries no user data.

We can define one more type of gain in wireless communication systems. The array gain is gain obtained by processing at the transmitter and the receiver. Array gain gives better–received SNR, similarly to the diversity gain, but only if the CSI is perfect.

Chapter 3

Capacity of the Communication Channel

In this chapter, we discuss the capacity performance of MIMO systems. We assume the receiver has the information about the channel, $\mathbf{r}$ and distributions of $\mathbf{H}$ and $\mathbf{x}$ are known. Then, the capacity is a random variable dependent only on the channel matrix. The capacity of the MIMO system is derived using Shannon capacity formula and comparison with other scenarios as Single–Input Single–Output (SISO), Multiple–Input Multiple–Output (MISO), and Single–Input Multiple–Output (SIMO) is discussed as well.

3.1 Capacity of the AWGN Channel

When we study the capacity of the MIMO channel, we have to start with Shannon's formula for the theoretical maximum transmission rate of the channel with additive white Gaussian noise given by [4]:

$$C = \log_2 (1 + \rho), \tag{3.1}$$

where $\rho \coloneqq \overline{P}/(N_0 B)$ is the per complex degree of freedom, N_0 is a noise power spectral density, B is bandwidth, and $\overline{P}$ is a power constraint. This can be considered as SISO scenario, and the capacity defines maximum achievable channel capacity in bit/s/Hz as a function of SNR. This maximal rate is the way to achieve reliable communication through the channel while the probability of the error drives to zero [4].

3.2 Capacity of the MIMO Channel

We assume same transmission model of the channel as in Section 2.5, there is the total number of $N_\mathrm{r} N_\mathrm{t}$ paths between transmitter and receiver as illustrated in Fig. 3.1. However, we use equivalent transformation of the channel converting this MIMO channel to n SISO parallel orthogonal channels, where $n = \min(N_\mathrm{r} N_\mathrm{t})$.

Then, the capacity is given by the summation of capacities of the SISO sub–channels and can be calculated using channel eigenvalues.

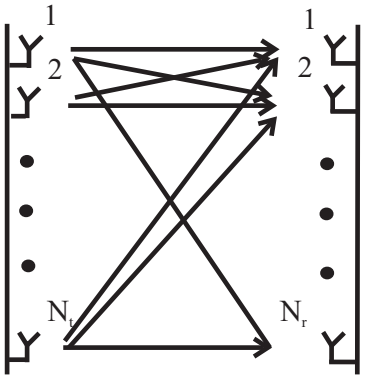

Figure 3.1: The MIMO channel.

We use Singular Value Decomposition (SVD) to decompose $\mathbf{H}$ to its eigenvalues, where we use Hermitian matrix (conjugate transpose). The SVD defines channel matrix $\mathbf{H}$ with dimensions $N_\mathrm{r}\times N_\mathrm{t}$ as follows:

$$\mathbf{H} = \mathbf{U}\mathbf{D}\mathbf{V}^\mathrm{H}, \tag{3.2}$$

where $\mathbf{U}, \mathbf{V}$ are unitary matrices of eigenvectors:

- $\mathbf{U}$ – dimension $N_\mathrm{r}\times N_\mathrm{t}$, $\mathbf{U}^\mathrm{H}\mathbf{U} = \mathbf{I}$, column $\mathbf{u}_i$ is eigenvector of $\mathbf{H}\mathbf{H}^\mathrm{H}$
- $\mathbf{V}$ – dimension $N_\mathrm{t}\times N_\mathrm{r}$, $\mathbf{V}^\mathrm{H}\mathbf{V} = \mathbf{I}$, column $\mathbf{v}_i$ is eigenvector of $\mathbf{H}^\mathrm{H}\mathbf{H}$,

where $\mathbf{D}$ is $N_\mathrm{m}\times N_\mathrm{m}$ diagonal matrix of eigenvalues of the channel, where $N_\mathrm{m} = \min(N_\mathrm{r}, N_\mathrm{t})$. Conjugate transpose is denoted by superscript H, $\mathbf{A}^\mathrm{H}$, and matrix is called Hermitian, if $\mathbf{A}^\mathrm{H} = \mathbf{A}$. For Hermitian matrix applies, that the eigenvalues are always real, non–negative, and has orthonormal eigenvectors. These eigenvalues are equal to the square of the root of the eigenvalues of the matrix $\mathbf{H}\mathbf{H}^\mathrm{H}$:

$$\mathbf{D} = \mathrm{diag}\left(\sqrt{\lambda_i}\right) \tag{3.3}$$

$$\lambda_i = \mathrm{eig}\left(\mathrm{H}\mathrm{H}^\mathrm{H}\right). \tag{3.4}$$

The above shown decomposition is used for equivalent transformation to the sub–channels as follows: we have our channel defined in (2.12) and with using SVD defined in (3.2) we get

$$\mathbf{r} = \mathbf{U}\mathbf{D}\mathbf{V}^\mathrm{H}\mathbf{x} + \mathbf{n}. \tag{3.5}$$

Now we get rid of the unitary matrices

$$\mathbf{U}^\mathrm{H}\mathbf{r} = \mathbf{U}^\mathrm{H}\mathbf{U}\mathbf{D}\mathbf{V}^\mathrm{H}\mathbf{x} + \mathbf{U}^\mathrm{H}\mathbf{n}. \tag{3.6}$$

We denote $\mathbf{U}^{\mathrm{H}}\mathbf{r} = \mathbf{r}'$, $\mathbf{V}^{\mathrm{H}}\mathbf{x} = \mathbf{x}'$, $\mathbf{U}^{\mathrm{H}}\mathbf{w} = \mathbf{n}'$ and since $\mathbf{U}$, $\mathbf{V}$ are unitary matrices, it applies $\mathbf{U}^{\mathrm{H}}\mathbf{U} = \mathbf{I}$, $\mathbf{V}^{\mathrm{H}}\mathbf{V} = \mathbf{I}$. Using this we can define equivalent parallel channels as follows:

$$\mathbf{r}' = \mathbf{D}\mathbf{x}' + \mathbf{w}', \tag{3.7}$$

where every component $\mathbf{r}'$ depends only on one component of the $\mathbf{x}'$ as shown in Fig. 3.2 [5] .

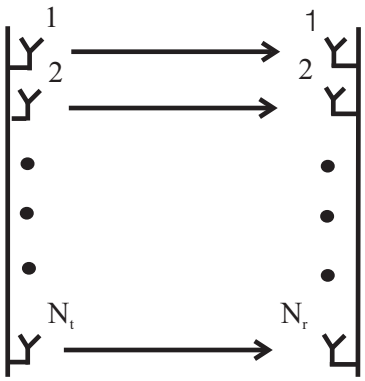

Figure 3.2: The MIMO channel transformed to sub–channels.

As a result we have N_{m} sub–channels with the same amount of eigenvalues λ_i where only first N_H (rank of the channel matrix $\mathbf{H}$) are non–zero. The total capacity of the N_m sub–channels is simply given by the sum of the single capacities as follows:

$$C_{\mathrm{MIMO}} = \sum_{i=1}^{N_H} \log_2 \left(1 + \frac{\lambda_i P_{\mathrm{s}}}{N_{\mathrm{t}} P_{\mathrm{w}}}\right), \tag{3.8}$$

where P_{s} is total transmitted power, $P_{\mathrm{s}}/N_{\mathrm{t}}$ is power at one transmitting antenna, and P_{w} is noise power at one receiving antenna. In special case, when $N_{\mathrm{t}} = N_{\mathrm{r}}$, channel matrix $\mathbf{H}$ has full rank $N_{\mathrm{H}} = N_{\mathrm{r}}$ and equal power at all receivers. Under the assumption of channel normalization (each RX receives full TX power), the trace of $\mathbf{H}\mathbf{H}^{\mathrm{H}}$, which is the sum of the elements on the main diagonal is given by [5]

$$\mathrm{tr}(\mathbf{H}\mathbf{H}^{\mathrm{H}}) = \sum_{i,j} \mid h_{ij} \mid^2 = N_{\mathrm{r}} N_{\mathrm{t}} = \sum_i \lambda_i = N_{\mathrm{r}}\lambda. \tag{3.9}$$

Since $\lambda = N_{\mathrm{t}}$ we can define channel capacity for this case as follows:

$$C = N_{\mathrm{H}} \log_2 \left(1 + \frac{\lambda P_{\mathrm{s}}}{N_{\mathrm{t}} P_{\mathrm{w}}}\right) = N_{\mathrm{r}} \log_2 \left(1 + \frac{P_{\mathrm{s}}}{P_{\mathrm{w}}}\right). \tag{3.10}$$

In this case, the capacity is increasing linearly with the number of antennas without increasing the input power as was discussed in Section 2.4. Deriving the (3.8) for MIMO capacity according to [5] we get alternative matrix form of the capacity formula given by

$$C_{\mathrm{MIMO}} = \log_2 \det\left(\mathbf{I} + \frac{P_{\mathrm{s}}}{N_{\mathrm{t}} P_{\mathrm{w}}} \mathbf{H}\mathbf{H}^{\mathrm{H}}\right). \tag{3.11}$$

3.3 Capacity Comparison

In this section, we compare the ergodic capacity of the channel in bits per channel usage. We compare these four scenarios:

- SISO (1,1)
- MISO $(N_{\mathrm{t}}, 1)$
- SIMO $(1, N_{\mathrm{r}})$
- MIMO $(N_{\mathrm{t}}, N_{\mathrm{r}})$

In all cases we assume same conditions as in the previous section related to MIMO channel capacity. Firstly, SISO channel capacity calculated using (3.8) for $\mathrm{N_H} = 1$, $\mathrm{N_t} = 1$, $\lambda = 1$ is defined as follows:

$$C = \log_2 (1 + \rho), \tag{3.12}$$

where $\rho = P/P_{\mathrm{w}}$ is the SNR at the receiver input. This capacity is the same as basic Shannon formula and was discussed before.

MISO systems use transmitter diversity, but do not have any advantage in comparison to the SISO case. The channel capacity is given by the same formula.

When we use receiver diversity, that is the SIMO case. The capacity is given by

$$C = \log_2 (1 + N_{\mathrm{r}} \rho). \tag{3.13}$$

We get an advantage when capacity is growing with the logarithm of the number of receiving antennas and improve the SNR proportionally to the number of antennas.
Finally, the capacity of the MIMO channel we discussed in the previous text and is defined in (3.11).

Chapter 4

Simulations

Based on the knowledge gathered throughout the thesis, we will propose the measurement setup for the estimation of the quality of the wireless propagation inside buildings for the MIMO systems.

Prior to the measurement in a real scenario, a simple simulation of 2×2 MIMO was performed, and the SVD algorithm was utilized to calculate the capacity and determine the radiation pattern of the RX and TX arrays. Then the measurement in the anechoic chamber was realized to validate the simulation.

4.1 State–Of–The–Art of MIMO Capacity Estimation

In this section, a brief summary of previous MIMO channel capacity measurements is discussed.

4.1.1 Development of a 60 GHz MIMO Radio Channel Measurement System, S. Ranvier et al.

One of the first complex measurement systems providing research for future communication systems was published in [6]. The measurement of a wide–band MIMO channel on 60 GHz was conducted using channel sounder developed at Helsinki University of Technology. The channel impulse response is obtained as follows [7]:

$$h(\tau, t) = \mathrm{IFFT}\left(R(f)\, S^{*}(f)\right), \tag{4.1}$$

where $R(f)$ and $S(f)$ are Fourier transforms of the received and transmitted signals, respectively. The 14 GHz synthesizer was used for synchronization and to avoid phase drifts between TX and RX.

The Line–Of–Sight (LOS), obstructed LOS and Non–Line–Of–Sight (NLOS) measurements were performed. For both LOS configurations, the antenna arrays were placed in the room. The distance between TX and RX arrays were set to 3.2 meters, and the spacing of the array elements was set to $l/4$ to reduce the spurious emission. The obstacle in the obstructed LOS case was a cubical absorber with half a meter side placed right in the middle between TX and RX and blocked the direct LOS. The NLOS scenario, the TX antenna array was placed in the room, and the RX antenna array was placed in the corridor. The spacing between the elements was set to $l/2$. The main concern of this paper is capacity. The capacity C in bit/s/Hz for NLOS case is obtained using normalized correlation matrix as in [8]:

$$\overline{\mathbf{R}}_{\text{norm}} = \frac{\overline{\mathbf{H}}^{\text{H}}\overline{\mathbf{H}}}{\frac{1}{N_{\text{t}}N_{\text{r}}}\text{E}\left\{\sum_{t=1}^{N_t}\sum_{r=1}^{N_r}\mathbf{H}_{r,t}^{*}\mathbf{H}_{r,t}\right\}}, \tag{4.2}$$

where E is expectation operator and $\mathbf{H}$ in the denominator is a complex channel matrix obtained removing the noise from the channel matrix and the overline operator in the numerator means coherent summation in the delay domain. The channel matrix was normalized by removing the average path loss from the matrix. The capacity is then calculated under assumption of equal power distribution on each TX as [8]:

$$C = \log_2\left[\det\left(\mathbf{I} + \frac{\rho}{n_{\text{t}}}\overline{\mathbf{R}}_{\text{norm}}\right)\right], \tag{4.3}$$

where $\mathbf{I}$ is the identity matrix, ρ is a SNR, and n_{t} is number of transmitting antennas.

The results were presented in a form of capacity Cumulative Distribution Function (CDF) curves for several different SNRs and compared with the capacity Independent Identically Distributed (IID) MIMO Rayleigh channel. The measured results were recognized as very similar to the theoretical Rayleigh channel. However, the mean capacity, which is increasing with increasing SNR is slightly lower for each SNRs in a comparison to Rayleigh.

4.1.2 Experimental Channel Parameters and Capacity Measurement of the Wireless MIMO Channel at 2.4 GHz, A.A. Kalachikov et al.

Slightly different approach of calculating capacity is presented in [9]. The use of channel frequency response is utilized as the Fourier transform of (2.7) [9]:

$$\mathbf{H}\left(t,f\right)=\sum_{j=1}^{J}\alpha_{j}\left(t\right)e^{-j2\pi f\tau_{j}}. \tag{4.4}$$

In practice, the frequency response was obtained as [9]:

$$\mathbf{H}\left(t,f\right)=\frac{\mathbf{Y}\left(t,f\right)}{\mathbf{X}\left(f\right)}, \tag{4.5}$$

where $\mathbf{Y}\left(t,f\right)$ and $\mathbf{X}\left(f\right)$ are spectrum of the received signal and spectrum of the transmitted signal, respectively. The capacity of the MIMO channel is then calculated under the same assumption as on the previous paper (equal power distribution) as follows [9]:

$$C\left(t,f\right)=\log_{2}\left(\det\left(\mathbf{I}+\frac{\rho}{n_{\mathrm{t}}}\mathbf{H}(t,f)\mathbf{H}^{\mathrm{H}}(t,f)\right)\right), \tag{4.6}$$

where $\mathbf{H}(t,f)$ is normalized channel matrix for frequency f. The normalization is used to compare the channel for different SNR as a parameter.

The results are presented using capacity distribution functions subtracting a mean value. Mean capacity was obtained as an average of multiple snapshots. The dependency of the capacity on the number of TX and RX was shown, and the increasing capacity dependence on the increasing SNR was shown as well.

4.1.3 Spatial Correlation and Capacity Measurements for Wideband MIMO Channels in Indoor Office Environment, L. Kafle et al.

Both previous papers have been focused on the flat–fading model of the channel and estimating the channel capacity of the channel based on the RF measurements. In [10], the frequency selective channel model is validated. The channel matrix $\mathbf{H}\left(\tau\right)$ of the frequency selective MIMO fading channel is defined as follows [10]:

$$\mathbf{H}\left(\tau\right)=\sum_{l=0}^{L-1}\tilde{\mathbf{H}}_{l}\delta\left(\tau-\tau_{l}\right). \tag{4.7}$$

The $\tilde{\mathbf{H}}$ is the complex channel matrix with the fading coefficients for the given delay τ_l. The L is defined by the number of significant MultiPath Components (MPCs). The

significant MPCs were counted up from the Power Delay Profile (PDP) calculated as [3]:

$$P_h(\tau) = \lim_{T\to\infty} \frac{1}{2T} \int_{-T}^{T} \mid h(t,\tau) \mid^2 \mathrm{d}t. \tag{4.8}$$

Firstly, maximum excess delay determined as in [11] is the time difference between the time when the first MPC is received and the time when the last MPC above given threshold is received. In the paper, the threshold was set to 25 dB below the strongest path. The delay resolution was determined as 5 ns. The number of significant MPCs varied depending on the scenario. For the frequency selective channel the (4.6) was modified, so all the frequencies are integrated over the bandwidth of interest B [10]:

$$C = \frac{1}{B} \int_{B} \log_2 \mathrm{det} \left(\mathbf{I} + \frac{\rho}{N_\mathrm{t}} \mathbf{H}^\mathrm{H}(f)\, \mathbf{H}(f) \right) \mathrm{d}f \qquad [\mathrm{bit/s/Hz}], \tag{4.9}$$

where $\mathbf{H}(f)$ is frequency–dependent channel matrix. The results of the measurement at a central frequency of 5.66 GHz at a bandwidth of 200 MHz for 15 dB SNR were presented as complementary CDF curves of the capacity. The selected CDF curves for NLOS and LOS case were published. The capacity was compared to the keyhole capacity as the lower bound and ideal IID Rayleigh channel as the upper bound. Keyhole capacity is the scenario where between TX and RX screen with a small keyhole and the radio wave can go through only through this keyhole, more on this in [12]. It was observed that capacity significantly decreases in the LOS case as the corridor environment lacks the MPCs. In the NLOS case, the mean capacity increases with the element spacing and approaches to the upper bound capacity.

4.1.4 Conclusion for the State–Of–The–Art

When we compare the papers, we see that the main difference lies in obtaining the channel matrix. Channel matrix is obtained either in the time domain or in the frequency domain. Therefore, the estimation of the capacity is different as well. As for our purposes, the time domain is chosen. All the papers presented in the previous sections were focused on measurements, where both the environment and antennas were static. Since the real communication systems are not static in the majority of the time, we have found this as the key disadvantage. We would like to focus on the measurement of a dynamic environment. Similarly, the papers are focusing on both LOS and NLOS scenarios; the LOS is nevertheless rare within the modern mobile communication systems. Therefore, we mainly focus on the NLOS scenarios. Finally, all the papers present the results as a dependence on SNR, which we found suitable for our measurements as well.

4.2 Simulation

The simulation and following measurement in the anechoic chamber are set to be the first encounter with the SVD technique utilized in the estimation of the MIMO channel capacity. The SVD algorithm is a powerful computational tool from linear algebra and is used in MIMO systems to determine for every channel matrix its matrices of orthogonal eigenvectors and diagonal matrix with its eigenvalues.

The simplified simulation follows the idea about 2×2 MIMO on central frequency of 2.45 GHz. The spacing between the antennas is set to $l/2$ as it is proposed in the real measurement scenario. The simulation and the subsequent measurement in the anechoic chamber follow geometry shown in Fig. 4.1. The propagation of the electromagnetic field

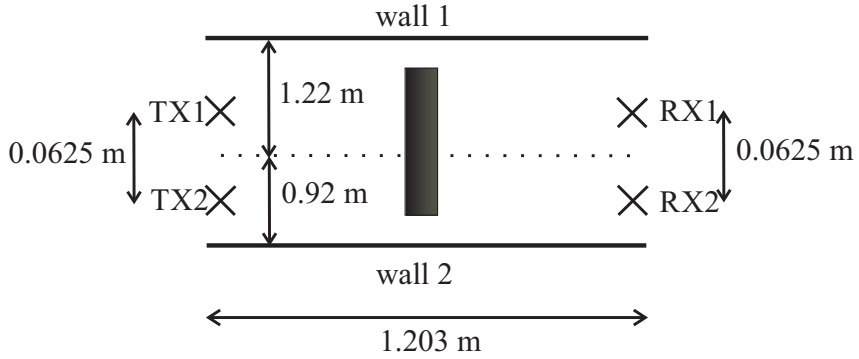

Figure 4.1: Schematic scenario of the simulation.

between TX and RX antennas is assumed to be only by the reflection of the walls, no LOS propagation is considered. The distance of the walls from the axis of the antenna arrays is different for every wall to show different behavior of the signal propagation.

Simple ray tracing using the image method is utilized. Two significant rays between each TX and RX are used to get the channel matrix **H** as it is shown in Fig. 4.2. The

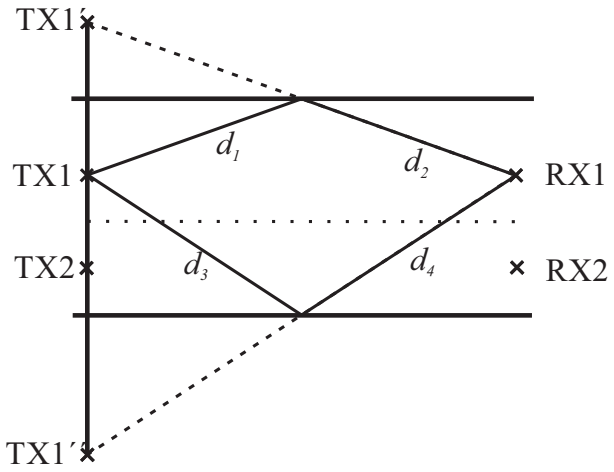

Figure 4.2: Ray–tracing method.

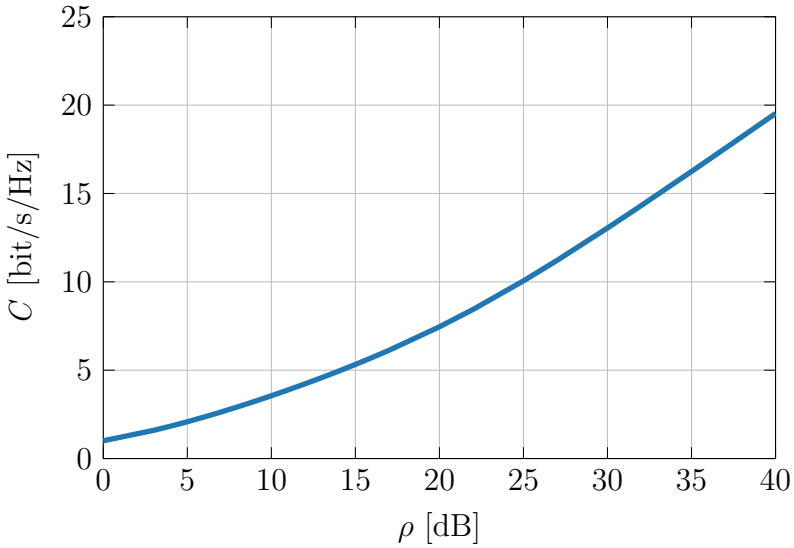

Figure 4.3: Capacity vs. SNR.

figure illustrates only two path rays of eight rays in total between the antennas. The transmission between those two antennas is defined as:

$$H\left(1,1\right)=R\left(\sqrt{\frac{PG_{\mathrm{TX1}}G_{\mathrm{RX1}}}{FSL\left(r_1\right)}}e^{-jk_cr_1}+\sqrt{\frac{PG_{\mathrm{TX1}}G_{\mathrm{RX1}}}{FSL\left(r_2\right)}}e^{-jk_cr_2}\right), \tag{4.10}$$

where $R=-1$ is reflection coefficient for well conductive surface P is the transmitted power, G_{TX1} and G_{RX1} are the gains of the TX1 and RX1 antenna respectively, $k_c=2\pi/l$ is the wavenumber, Free Space Loss (FSL) at given distance is denoted by FSL, $r_1=d_1+d_2$ and $r_2=d_3+d_4$ are the lengths of the rays. Then, the 2×2 channel matrix $\mathbf{H}$ is the transmission matrix between each transmitting and receiving antenna.

Firstly, we calculate the capacity of the channel between TX and RX according to (3.11) with convenient normalization:

$$C_{\mathrm{MIMO}}=\log_2\det\left(\mathbf{I}+\frac{\rho}{N_r}\mathbf{H}_{\mathrm{norm}}\mathbf{H}_{\mathrm{norm}}^{\mathrm{H}}\right), \tag{4.11}$$

where superscript H is conjugate transpose and $\mathbf{H}_{\mathrm{norm}}$ is defined as follows:

$$\mathbf{H}_{\mathrm{norm}}=\frac{\sqrt{N_{\mathrm{r}}}}{\mathbf{H}_{\mathrm{Frobenius}}}\mathbf{H}. \tag{4.12}$$

The Frobenius norm of a matrix is defined as the Root Mean Square (RMS) value of its elements. This normalization is convenient because we want to vary SNR as a parameter in the the model. It was shown that the calculated capacity is not frequency dependent and its dependence on the SNR is shown in Fig. 4.3.

Then we apply the SVD on the channel matrix to obtain matrices **U**, **V** and **D** as it is shown in (3.2) and as it mentioned here again:

$$\mathbf{H} = \mathbf{U}\mathbf{D}\mathbf{V}^{\mathrm{H}}. \tag{4.13}$$

Orthogonal matrices **U** and **V** with same dimensions 2×2 are used to derive radiation patterns of the RX and TX antenna array. A radiation pattern is derived utilizing angular spectrum decomposition of plane waves [13]. The angular spectrum is used to represent the field at every point of space as an appropriate linear combination of plane waves. These plane waves are interfering in the far field making a radiation pattern that can be described by a single non–planar wave. The principle of calculating the intensity of such a wave in a single point in space is shown in Fig. 4.4. We sum both angular spectra propagating from the antennas in the array in the point of observation. We use 512 points to approximate the radiation pattern of every monopole used in the TX and RX array. We calculate the pattern in the distance of $d = (l + \text{spacing}/2)$ from the origin which is placed between the antennas in the array as it is shown in the figure as well. The radiation patterns are normalized to the isotropic radiator.

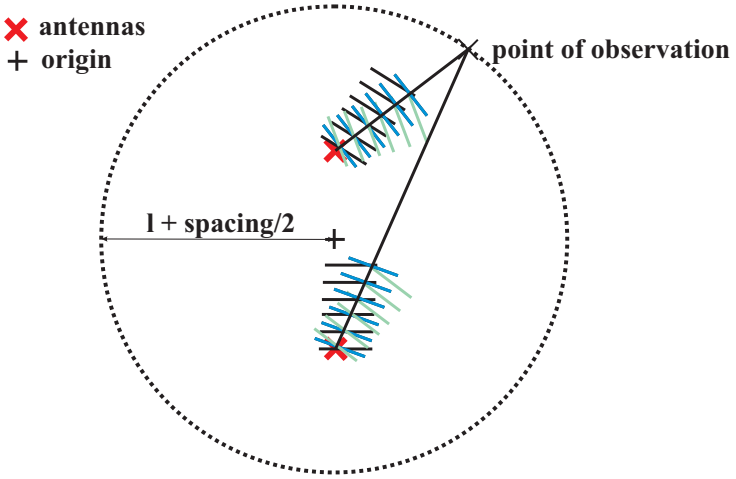

Figure 4.4: Radiation field calculation.

Let's assume the channel defined as in (2.12) with omitting the noise matrix:

$$\mathbf{r} = \mathbf{H}\mathbf{x}. \tag{4.14}$$

Using SVD and convenient modification we get the form used to determine the TX and RX radiation patterns:

$$\mathbf{U}^{\mathrm{H}}\mathbf{r} = \mathbf{U}^{\mathrm{H}}\mathbf{U}\mathbf{D}\mathbf{V}^{\mathrm{H}}\mathbf{x}. \tag{4.15}$$

As it is stated in (4.15), rows of the conjugate transpose of matrix **U** are used to determine RX pattern. Similarly, rows of the conjugate transpose of matrix **V** are used to determine

TX pattern. In our case, we assume:

$$\mathbf{x} = \begin{bmatrix} x_{11} & x_{12} \\ x_{21} & x_{22} \end{bmatrix} = \begin{bmatrix} 1 & 1 \\ 1 & 1 \end{bmatrix}, \mathbf{r} = \begin{bmatrix} r_{11} & r_{12} \\ r_{21} & r_{22} \end{bmatrix} = \begin{bmatrix} 1 & 1 \\ 1 & 1 \end{bmatrix},$$

and from SVD we get matrices of complex numbers:

$$\mathbf{U}^{\mathrm{H}} = \begin{bmatrix} u_{11} & u_{12} \\ u_{21} & u_{22} \end{bmatrix}, \mathbf{V}^{\mathrm{H}} = \begin{bmatrix} v_{11} & v_{12} \\ v_{21} & v_{22} \end{bmatrix}.$$

Then, we get radiation pattern for every RX antenna (RX1, RX2) in the array as well as radiation pattern for every TX antenna (TX1, TX2) in the array, calculating the field in the observation point X as follows:

$$E_{\mathrm{TX1}} = v_{11}x_{11}e^{(-jk|X-TX1|)} + v_{12}x_{21}e^{(-jk|X-TX2|)}, \tag{4.16}$$

$$E_{\mathrm{TX2}} = v_{21}x_{12}e^{(-jk|X-TX1|)} + v_{22}x_{22}e^{(-jk|X-TX2|)}, \tag{4.17}$$

$$E_{\mathrm{RX1}} = u_{11}r_{11}e^{(-jk|X-RX1|)} + u_{12}r_{21}e^{(-jk|X-RX2|)}, \tag{4.18}$$

$$E_{\mathrm{RX2}} = u_{21}r_{21}e^{(-jk|X-RX1|)} + u_{22}r_{22}e^{(-jk|X-RX2|)}, \tag{4.19}$$

The resulting patterns are shown in Figs. 4.5 and 4.6. Both patterns in the same array are orthogonal as the SVD is used to orthogonal decomposition. The patterns are complementary and fill the whole space. Since both metallic plates are not in the same distance, the patterns are not ideally symmetrical as they would be for the equal distance of both plates.

The utilization of the SVD in MIMO is illustrated in this section. Obtained matrices of eigenvectors $\mathbf{U}$ and $\mathbf{V}$, we can do proper pre–coding at the transmitter side to send the parallel data streams without interference between the sub–channels in the channel. Since the eigenvectors are orthogonal, the data are sent along these separate eigenchannels with minimum bit error rate. Then, the SVD is used on the receiver side to separate these eigenchannels properly.

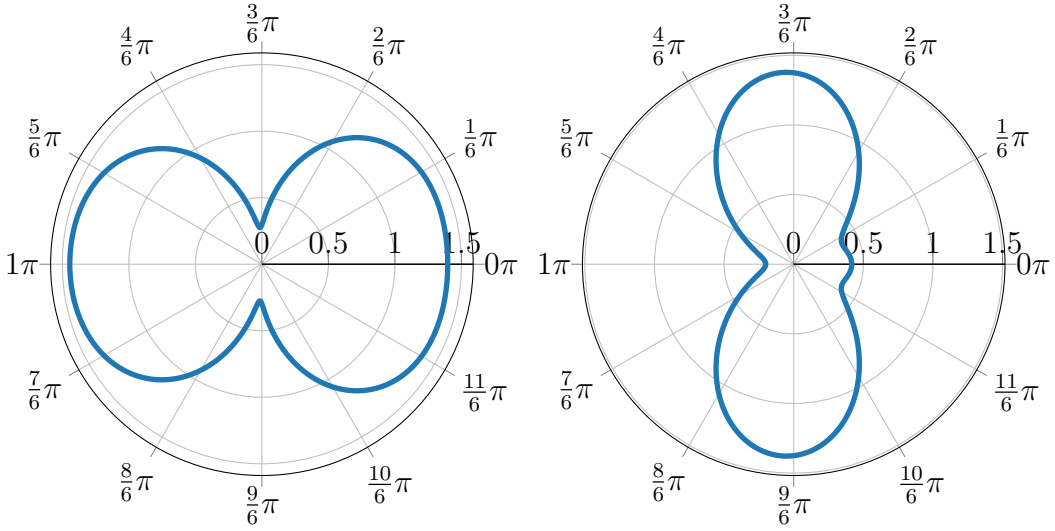

Figure 4.5: Patterns of the TX array.

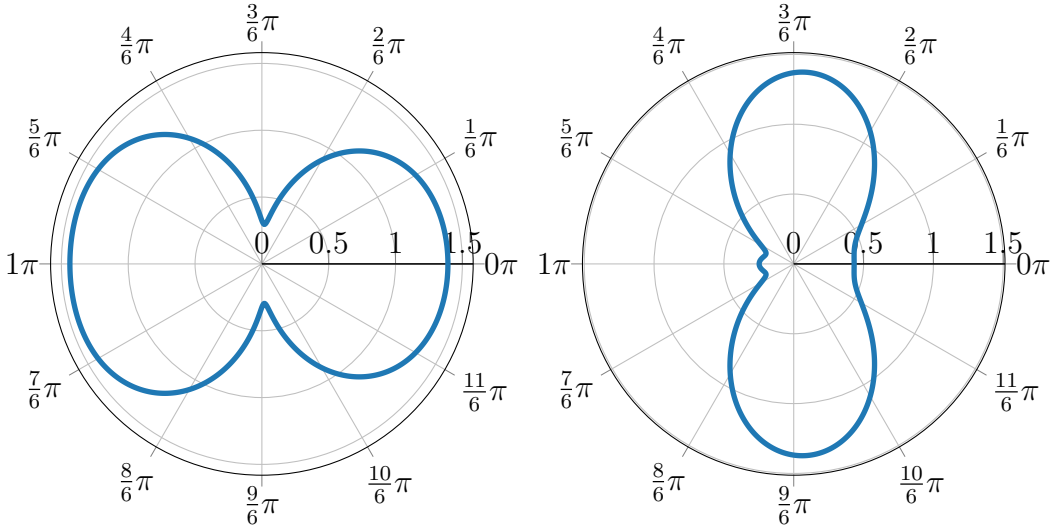

Figure 4.6: Patterns of the RX array.

Finally, the diagonal matrix $\mathbf{D}$ with dimensions 2×2 is used to calculate the channel capacity as the summation of the capacities of the sub–channels as in (3.8):

$$C_{\text{MIMO}} = \sum_{i=1}^{N_H} \log_2 \left(1 + \frac{\lambda_i P_{\text{s}}}{N_{\text{t}} P_{\text{w}}}\right), \tag{4.20}$$

The capacity calculated as the sum of the sub–channels and the generic capacity calculated using (3.11) are equal and was shown in Fig. 4.3. To maximize the sub–channel capacity for high SNR regimes, the eigenvalues supposed to be equal. In general, the less eigenvalues vary, the higher capacity is achieved. The dependence is described by the so–called condition number, defined as the ratio between the maximum and the minimum eigenvalue. Then the channel matrix $\mathbf{H}$ is called well–conditioned when the ratio equals

one. On the other hand, in the low SNR regime, only the strongest eigenchannel should be used to achieve maximum capacity [4].

4.3 Verification of the Simulation

Measurement should verify the results from the simulation and together with that simulation should make some improvements to proposed measurement in a real scenario. The measurement of the channel defined in the simulation was carried in the anechoic chamber at the Faculty of Electrical Engineering of Czech Technical University in Prague.

The measurement setup followed the same geometry as in Fig. 4.1, we used 4–port Vector Network Analyzer (VNA) R&S ZVA 67 to obtain all important s–parameters. The scheme of the measurement setup is shown in Fig. 4.7.

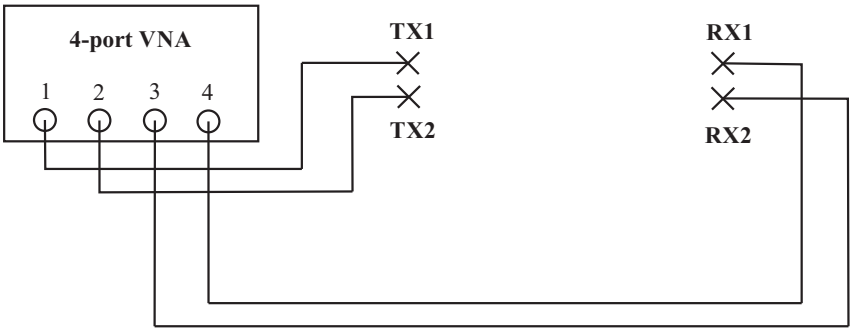

Figure 4.7: Scheme of the measurement setup.

Several blocks made from the absorbent material are placed between the TX and RX array to block the LOS, enabling the propagation only as of the reflection from the metallic plates utilized as the walls. The metallic plates had a size 60×120 cm, so we had to consider if there is enough reflected energy of the electromagnetic wave. The Fresnel zone between an antenna and its image version is a rotary ellipsoid. The ellipsoid is then "cut" by our metallic plate, and it projects the ellipse on the plate. In the case of perpendicular impact, the projection would be a circle. For the n^{th} Fresnel zone, the radius can be estimated using formula [14]:

$$r \approx \sqrt{\frac{nd_1d_2}{d_1+d_2}}, \tag{4.21}$$

where $d_1 + d_2$ is a distance between the antenna and its image. We take into account only the radius of the first Fresnel zone, since at least 60 % of the zone is considered to be sufficient for transmission of the significant amount of energy [14] and its radius is approximately fifty centimeters in our case.

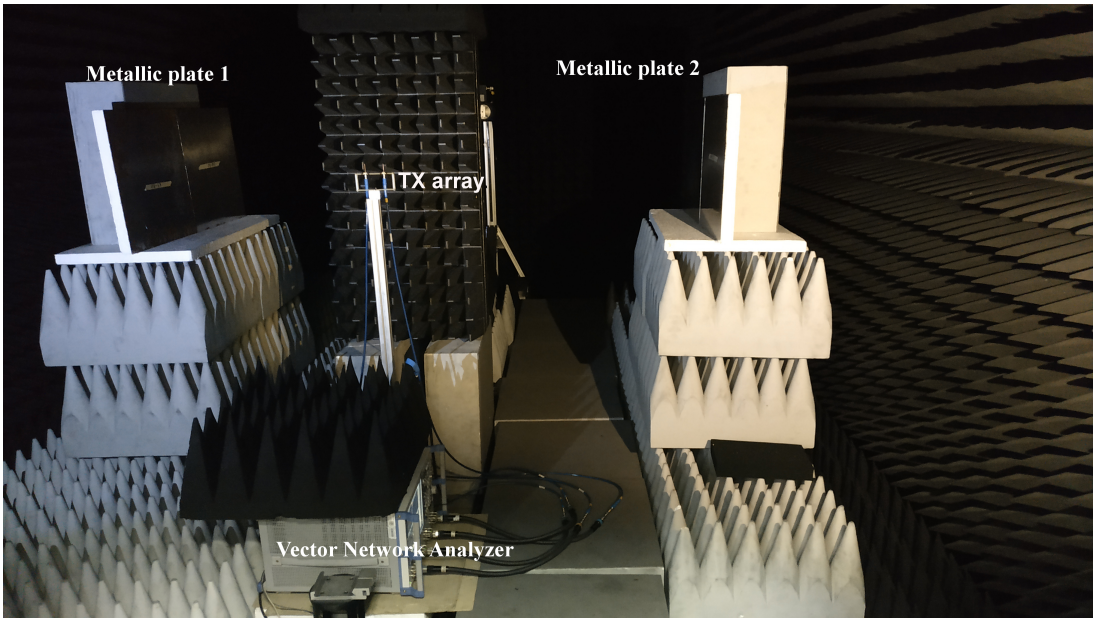

Figure 4.8: Real measurement setup.

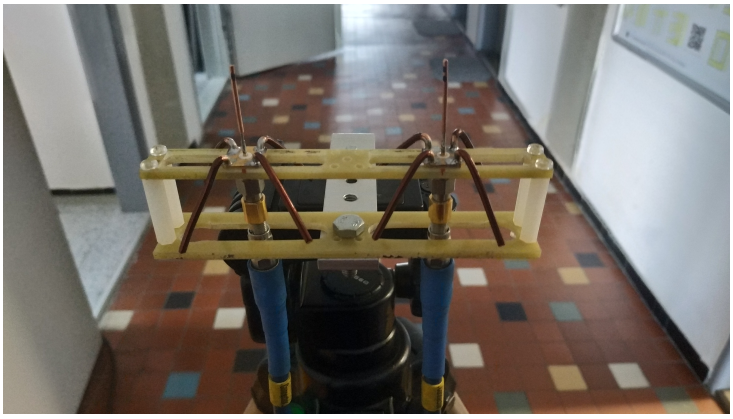

Figure 4.9: Antenna holder.

In the case of perpendicular impact, the size of the metallic plate would be sufficient. However, as we deal with a slant impact, the projection is an ellipse. We assume that with the increasing angle of impact, the length of the semi–minor axis equals the radius of the circle in case of perpendicular impact. However, the length of the semi–major axis increases with the increasing angle of impact. Therefore, the space of the ellipsoid increases as well. We have calculated the length of the semi–major axis in our case as approximately 68 centimeters, and since our metallic plate size in this dimension is 120 centimeters, we consider this condition as fulfilled. The photo of the real measurement setup is shown in Fig. 4.8.

An 2×2 array of monopole antennas at 2.45 GHz was utilized as TX and RX. We have manufactured all four antennas for our purposes and created a holder shown in Fig. 4.9 for the antennas to ensure that antennas have a fixed position in the geometry and to

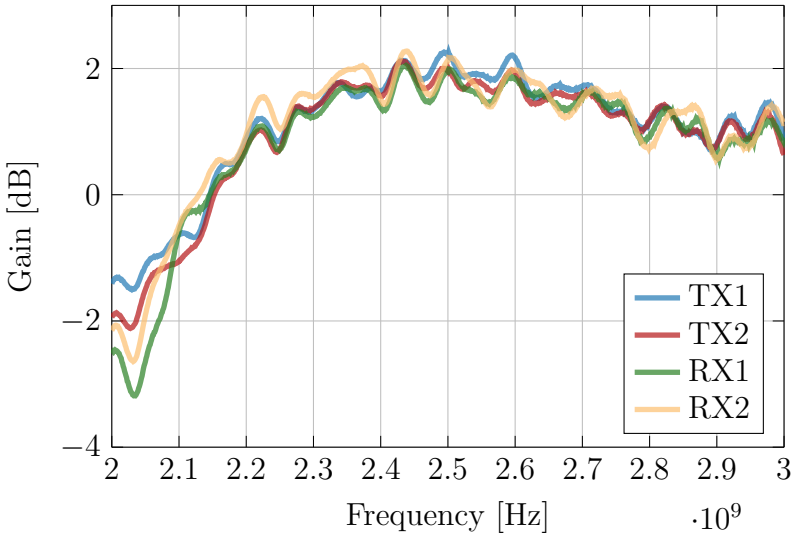

Figure 4.10: Gain of the antennas.

each other. We had to adjust all the antennas for the wanted frequency of 2.45 GHz, the obtained gain dependence on the frequency is shown in Fig. 4.10. The gain on the frequency of 2.45 varies between 1.96 dB to 2.09 dB as it is shown in Table 4.1.

Table 4.1: Antenna gains.

Antenna	Gain [dB]	Gain [–]
TX1	2.0	1.6
TX2	1.9	1.5
RX1	1.8	1.5
RX2	2.1	1.6

The transmission power was set to 10 dBm, and four significant s–parameters were obtained to construct **H** matrix. Then, the data processing was the same as in the simulation part. We have obtained radiation patterns for all the antennas and compared them to the patterns obtained from simulation. The results are shown in Figs. 4.11 and 4.12. As it is shown, the measured patterns correspond to the pattern from the simulation. The differences between the pattern obtained from the simulation and the measurement are caused by the inaccuracy of measuring the distance of the metallic plates and positioning them in general. In the simulation, we considered both metallic plates ideally parallel with the axis between the RX and TX antennas. However, the real metallic plates have not been fixed ideally like in the simulations. There could be an error in perpendicularity and the distance from the axis as well. We did a sensitivity analysis of the distance of the plates as it is shown in Fig. 4.13. We have defined the radiation patterns for three different distances, the ”center” distance, which was used in the original simulation and the ±3 cm on either side. As we can see, the differences are similar to the differences between the simulation and measured patterns mentioned before.

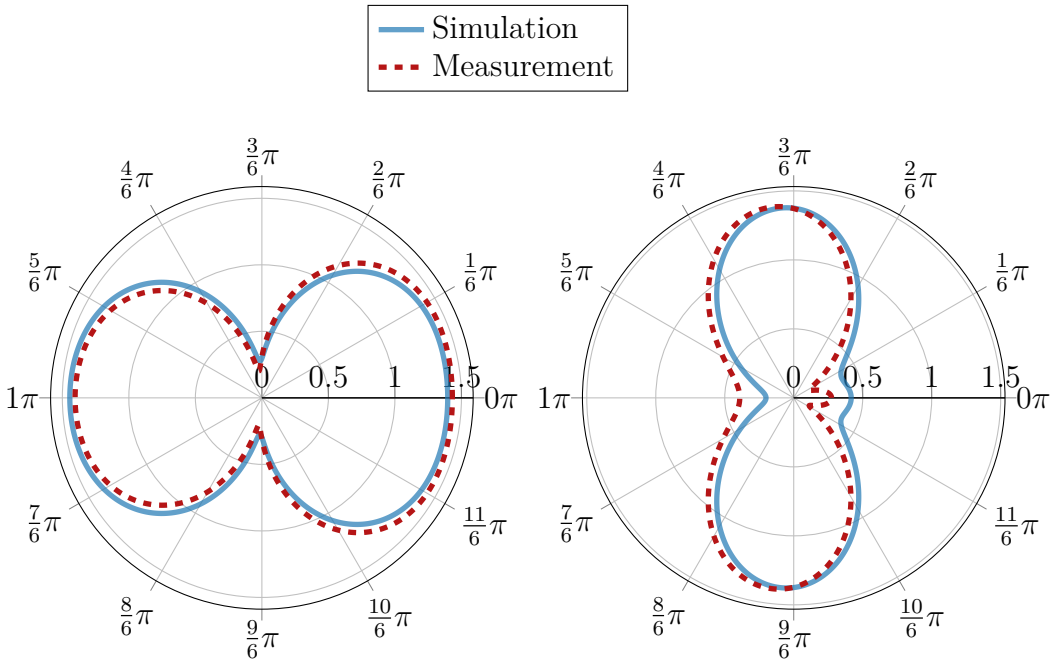

Figure 4.11: Patterns of the TX array.

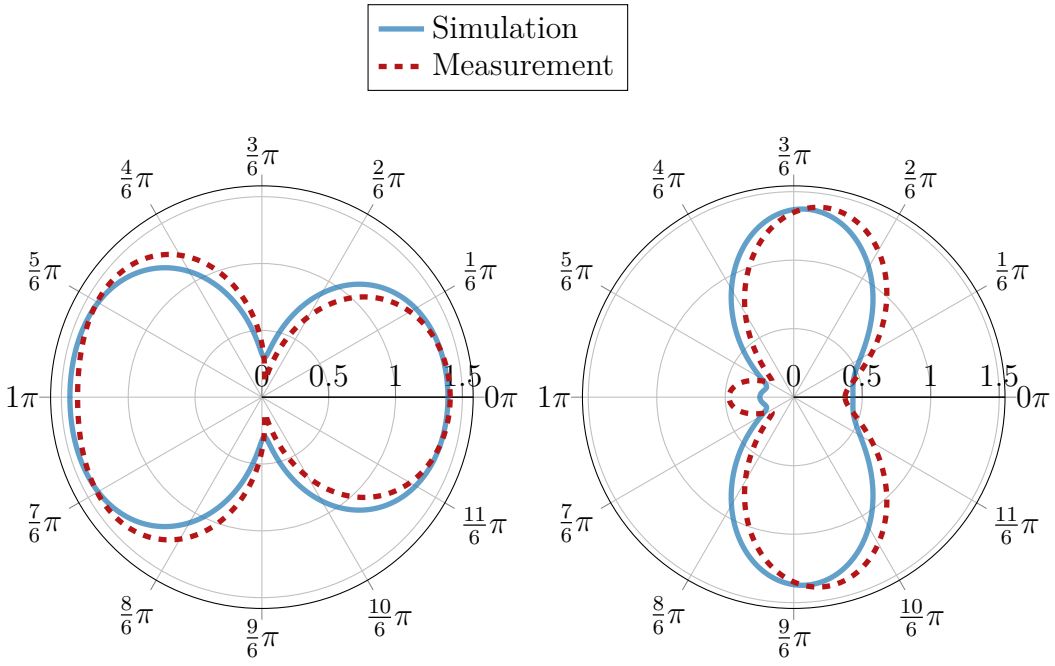

Figure 4.12: Patterns of the RX array.

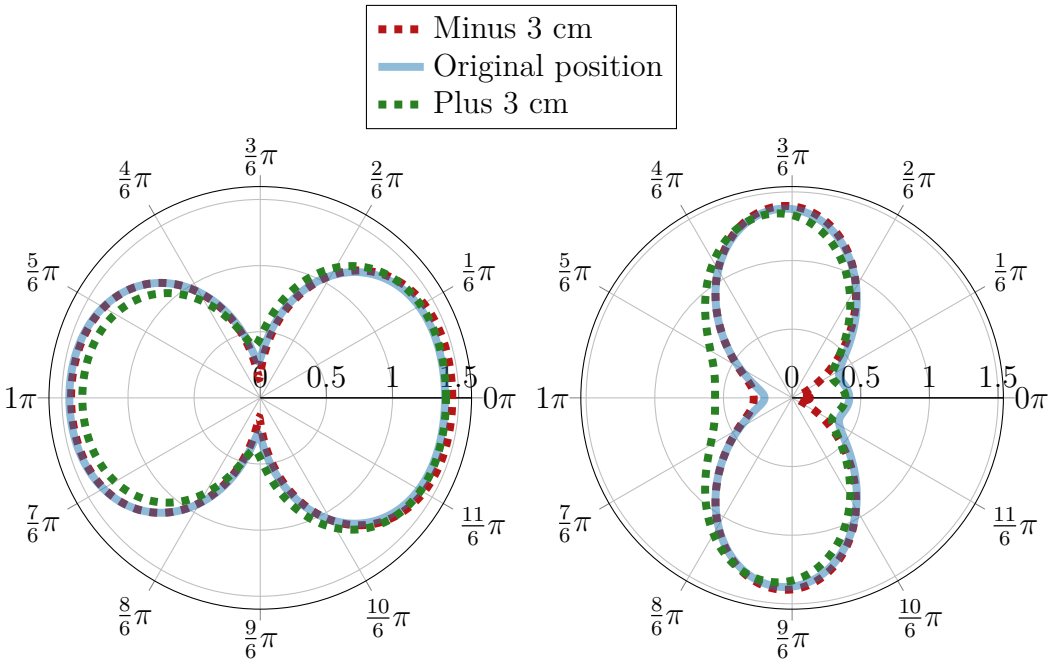

Figure 4.13: Sensitivity of the measurement–TX array.

As well as in the simulation part, we calculate the channel capacity from the measured data using SVD. The comparison of the capacities obtained in the previous text is shown in Fig. 4.14.

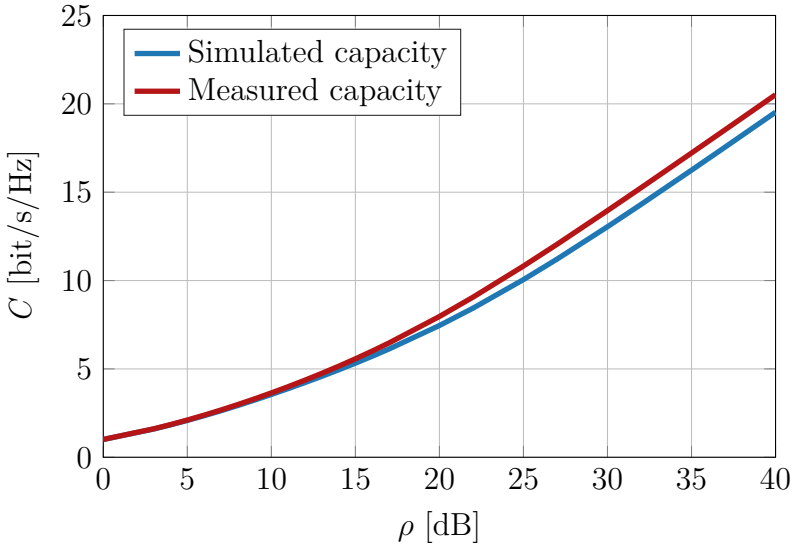

Figure 4.14: Capacity comparison.

Chapter 5

Measurements

The aim of this work is to study the MIMO channel capacity base on the eigenvalue decomposition of the channel matrix. Therefore, various measurements were performed to assess capacity. In this section, several measurements in the real scenarios are presented. The measurement should have been carried on WiFi frequency of 2.45 GHz as we were limited by the available equipment to go higher in the frequency range. However, as we have measured in the real environment, we had to shift the frequency to avoid interference with the real WiFi systems. Therefore, the central frequency was set to 2.484 GHz, which is the 14th channel of the WiFi frequency band, which is not being used anymore.

Three NLOS scenarios inside the building in total were performed, and the data were processed and interpreted. All the scenarios have different properties. Therefore, all the details are described in the following text for each of them separately. The measurement setup is the same as for the measurement in the anechoic chamber presented in Section 4.3, two antenna arrays utilized as the RX and TX and 4–port VNA to obtain all the necessary s–parameters. The measurement took place on the 6^{th} floor of the Faculty of Electrical engineering, Department of Electromagnetic Field, block B2.

5.1 Static Scenario

The first scenario is divided into two measurements–LOS case and NLOS case, mainly to compare radiation patterns and capacities with and without Line–of–sight between the antennas.

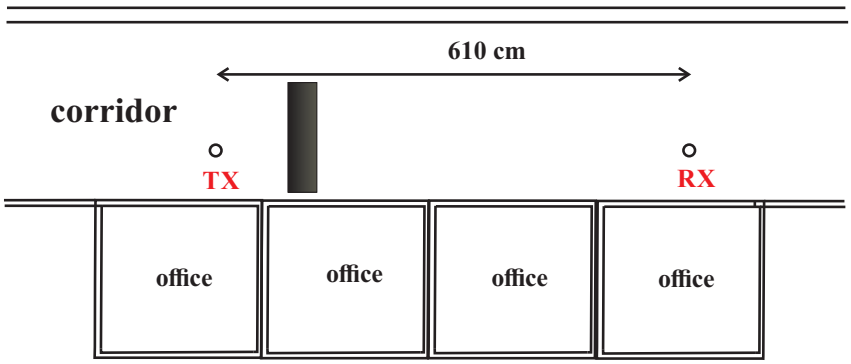

Figure 5.1: Measurement scenario–NLOS case.

The NLOS scenario is shown in Fig. 5.1. The RX and TX antennas are both placed in the corridor in a static environment. The LOS between the antennas is blocked by a wall in the distance of 1.5 meters. Since the wall is made of six 60×60 cm blocks made from the absorbent material, its dimensions are 180×120 cm. The LOS case differs only by no obstacle between the antennas. The distance between TX and RX is set to be 5.6 meters, mainly due to the limitations of the cables between the antennas and VNA. The photos of the real measurement setup are shown in Fig. 5.2.

Figure 5.2: Real measurement setup.

The measured data are processed the same way as in the simulation part. The SVD is applied to the obtained channel matrix **H** to estimate the channel capacity and radiation patterns. Firstly, we obtained the radiation patterns the same way as in the simulation part. The patterns for the LOS case are shown in Figs. 5.3 and 5.4. For both cases, there are completely different radiation patterns for each element in the TX array. These patterns of the monopole elements are kind of complementary to each other as they cover the whole space as a dipole in the end as it is expected from the simulation. The main lobes of the TX elements in the LOS are in a direction towards the RX antenna while the other pattern has the main lobe in the perpendicular direction using the reflections of the wall.

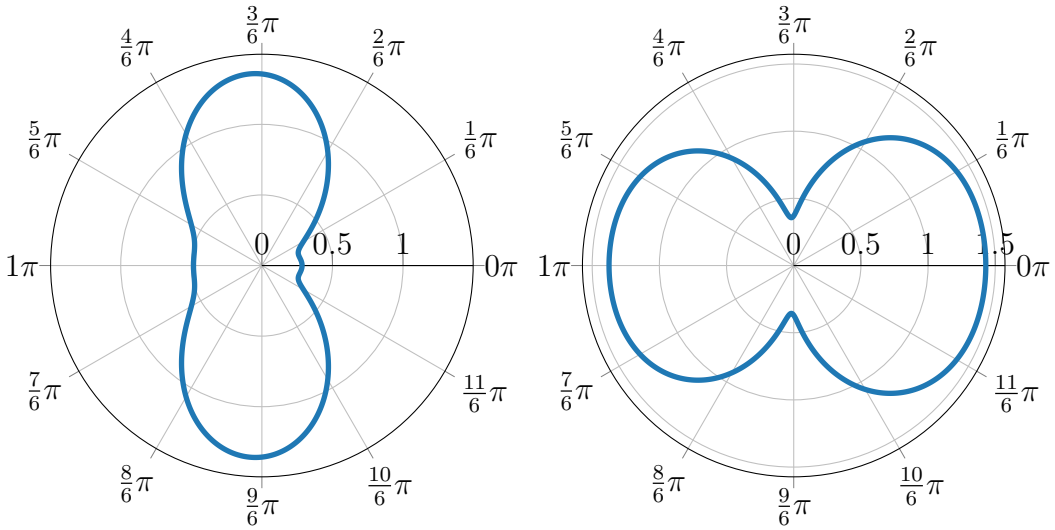

Figure 5.3: Pattern of the TX array–LOS case.

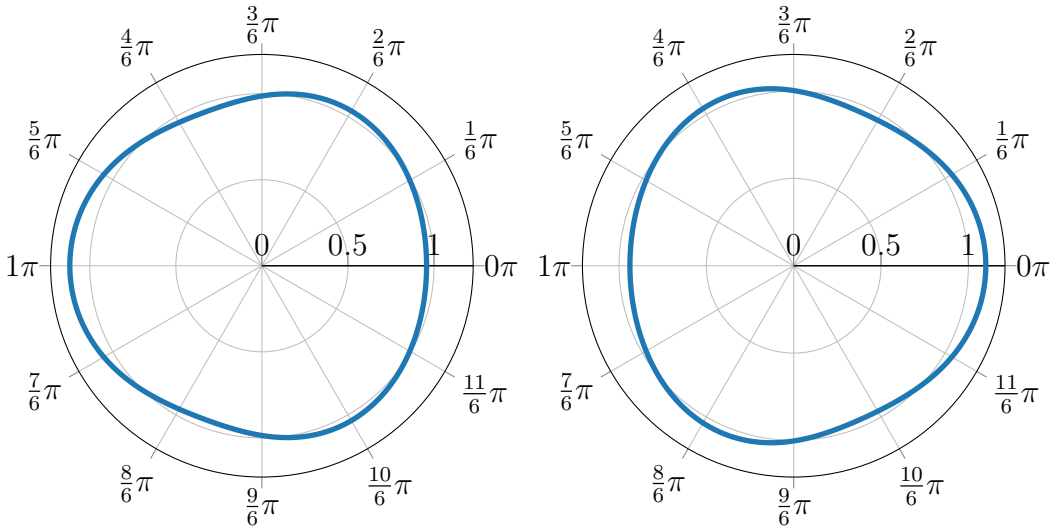

Figure 5.4: Pattern of the RX array–LOS case.

On the other hand, as it is shown in Figs. 5.5 and 5.6 for the NLOS case, the radiation from the two monopoles in the TX towards both walls of the corridor can be seen. Since the antennas were not placed in the middle of the corridor, but rather closer towards one of the walls, the patterns are not symmetrical.

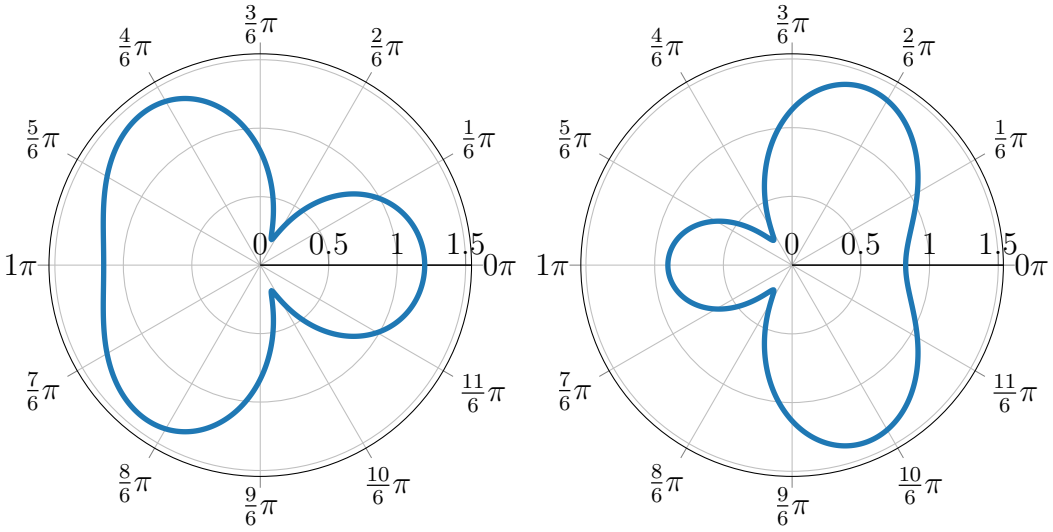

Figure 5.5: Pattern of the TX array–NLOS case.

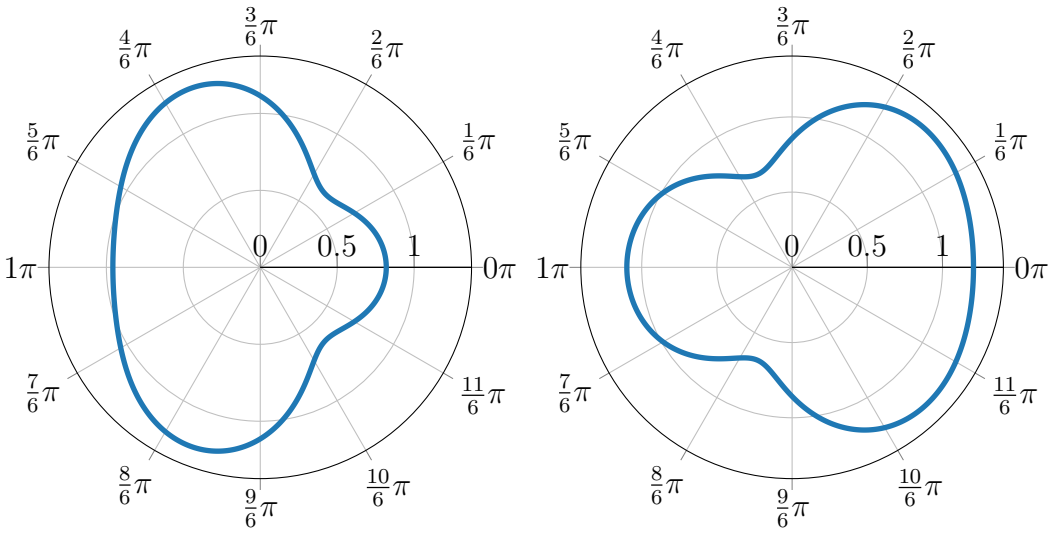

Figure 5.6: Pattern of the RX array–NLOS case.

The capacity of the channel is calculated using both generic formula (3.11) and (4.20). The calculated results of these two ways of capacity estimation are equal as expected. The capacity for both LOS and NLOS are presented with the SNR as the parameter, as it is shown in Fig. 5.7. The different transmitting power is defined to achieve the equal SNR parameter and compare the capacity afterwards. Therefore, the NLOS capacity is greater than the LOS capacity in the figure. In our case, the equal transmitting power is used for both LOS and NLOS scenarios. The achieved capacity in the LOS scenario is 15.07 bit/s/Hz for SNR = 30.52 dB. In the NLOS scenario, the cpacity is 13.78 bit/s/Hz for SNR = 25.53 dB. Both achieved capacities are illustrated in the figure as well. The achieved LOS capacity is higher than the NLOS capacity as it is expected. However, the difference is not significant, as the MIMO architecture using diversity and spatial multiplexing is utilized, and in the NLOS case offer higher gain in comparison the case of transmitting one symbol per one time slot.

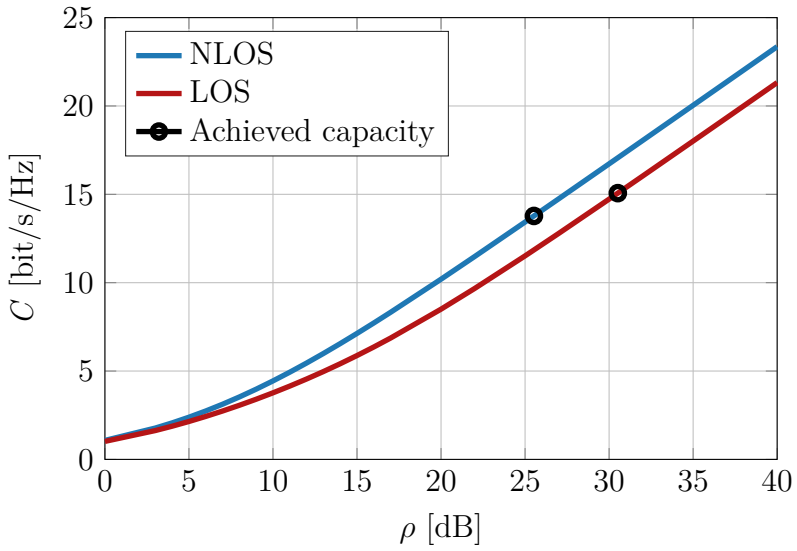

Figure 5.7: Measured capacity comparison.

5.2 Dynamic Scenario

The second scenario setup is the same as the previous one, but the environment was dynamic, with a movement between the antennas. The antennas were still in the corridor, there is no obstruction, and the dynamic environment was achieved by the movement of several volunteers between the antennas as it should simulate a crowded hallway. The scenario was measured many times; exactly 501 snapshots have been taken within the 4 seconds of the measurement. It allowed estimating the expected value of the capacity during long enough time when the hallway is full of moving objects (pedestrians). Thus, empirical distribution of the capacity is obtained in this scenario. The time to take one snapshot of the channel response is approximately 7.98 milliseconds and is considered to be short enough to consider even such environment as static.

As it was stated before, 501 snapshots were taken to get the expected value of the channel impulse responses. However, we firstly take every single snapshot and calculate the capacity of the channel within the snapshot to show the capacity statistics during the time. In this case, there is no normalization utilized to maintain the information about the change of the SNR between individual measurements. The SNR in our case is very high as the distance between the antennas is only few meters. Therefore, we have used usual receiver sensitivity of the WiFi routers of -93 dBm and as the noise level in the SNR in (4.11). Moreover, the maximum transmitting power of the WiFi system of 100 mW was taken into account. The histogram of the capacity in the snapshots is shown in Fig. 5.8. The capacity changes with the time as the movement differs between the snapshots. The mean value of the capacity calculated from the histogram is 36.83 bit/s/Hz for the SNR obtained from the given transmitted power and given noise floor; the standard deviation is 2.37 bit/s/Hz.

The channel matrix $\mathbf{H}$ was obtained as the expected value of the impulse responses over 501 snapshots measured by the VNA. The SVD was applied once again to estimation of the channel capacity. The histogram of the capacity does not follow Rayleigh or Ricean distribution, as the variations of amplitude of the channel impulse response are not Rayleigh or Ricean. If the variations will be one of these, the distribution of the SNR would be χ^2 and then the distribution of the capacity would be $C \sim \log_2\left(1 + \frac{1}{\rho}\chi^2\right)$. and would have only one maximum. The measured capacity is presented in Fig. 5.9.

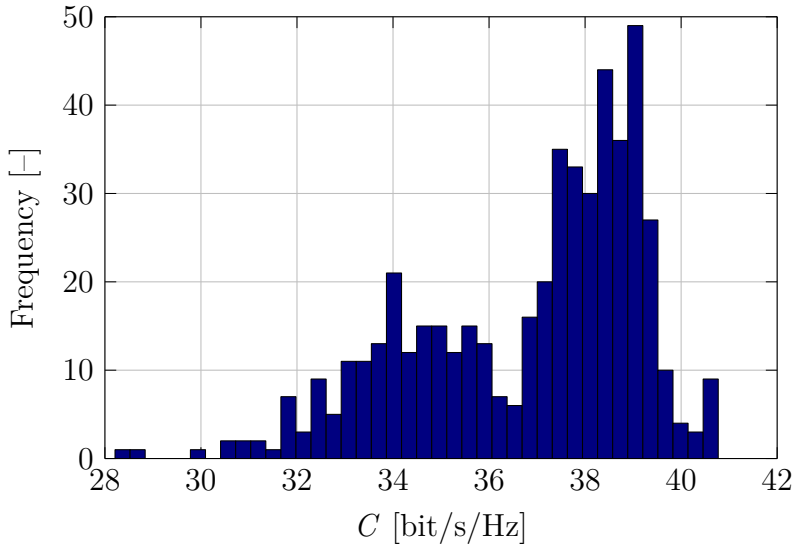

Figure 5.8: Histogram of the capacity.

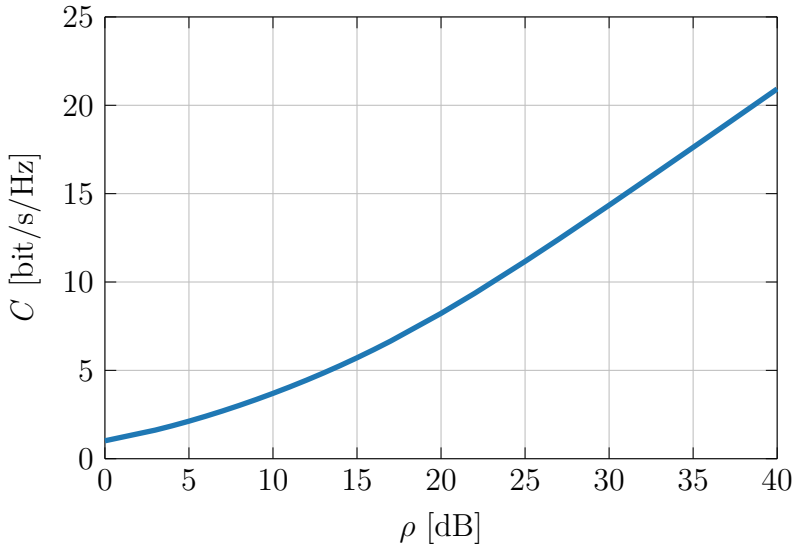

Figure 5.9: Measured capacity.

5.3 Quasi–Dynamic Scenario

The third scenario emulates a mobile user as it assumes one antenna placed statically at one place, while the other one is placed in several positions. In order to simulate the movement of the mobile station, the positions of the moving RX antenna are within the range of 5.6 meters with a step of 10 centimeters, so a total of 20 positions of the RX antenna is considered. The measurement scenario should illustrate the fluctuations of the capacity during the pedestrian movement with constant speed, and its scheme is shown in Fig. 5.10.

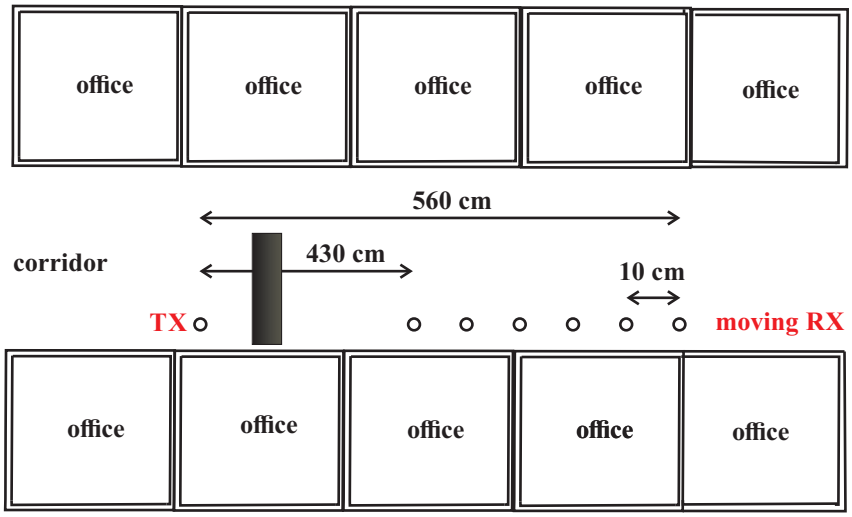

Figure 5.10: Measurement scenario.

The fluctuations are illustrated in the form of the histogram shown in Fig. 5.11. The histogram consists of 20 measurements as mentioned before. The properties of the data processing are same as in the section 5.2; no normalization, receiver sensitivity and maximal transmitting power. During the movement, the destructive interference occurs, resulting in the deep fades in the signal level and then in the lower channel capacity itself.

The histogram of the capacity in the snapshots is shown in Fig. 5.8. The capacity changes with the time as the movement differs between the snapshots. The mean value of the capacity calculated from the histogram is 38.82 bit/s/Hz for the SNR obtained from the given transmitted power and given noise floor; the standard deviation is 1.21 bit/s/Hz. The expected capacity estimated using the channel matrix $\mathbf{H}$ obtained as the matrix of expected values of the channel responses at each distance is shown in Fig. 5.12. The capacity of this scenario is lower then in the dynamic scenario in Section 5.2. It can be expected since the LOS in the dynamic scenario is not obstructed whole time as in the scenario in this section.

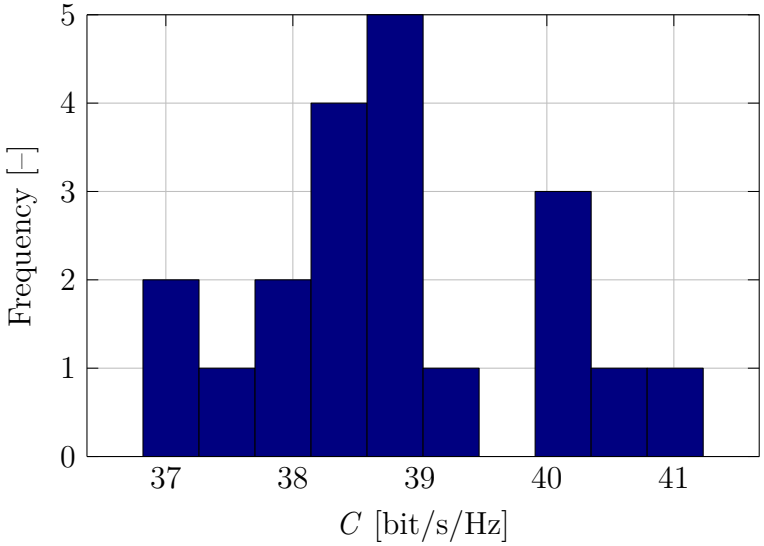

Figure 5.11: Histogram of the capacity.

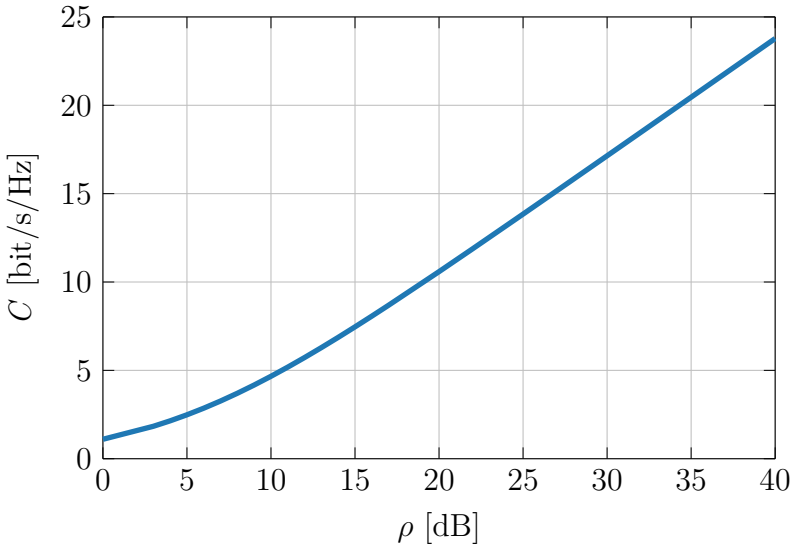

Figure 5.12: Measured capacity.

Chapter 6

Conclusions

We have studied the basic theory behind the MIMO systems used for wireless communications in an indoor environment with a focus on eigenvalue decomposition and its use for the channel capacity and wireless communication coding.

The second chapter shows the basic mechanisms in the wireless channel, especially related to the MIMO systems. Moreover, the model of the channel utilized in the whole thesis was presented in this section as well. The model is then used for decomposition of the MIMO channel into orthogonal parallel sub–channels and estimation of the MIMO capacity.

The third chapter is dedicated to the capacity of the MIMO channel, its estimation and comparison with the capacities of the non–MIMO systems. The concept of the Singular Value Decomposition (SVD) is explained, and its utilization in the MIMO capacity estimation is described in this section as well. The SVD is used to decompose the channel matrix to its eigenvalues and used to transform the interfering paths between the transmitter and receiver to parallel orthogonal sub–channels. The capacity is then given by a simple sum of the capacities in these sub–channels.

A research of the recent or older papers related to this topic and simulation part is presented in the fourth chapter. We became acquainted with similar measurement setups used for measurement–based estimation of the capacity. Several different approaches of the estimation were published in the papers. The estimation using a correlation matrix or using frequency channel impulse response can be found in these papers. Base on the obtained theoretical knowledge and research of the state–of–the–art in the capacity estimation, the simulation was proposed. The simulation of 2×2 MIMO was created and the SVD was utilized to get acquainted with this numerical tool of decomposition the channel matrix. We have estimated the capacity using the generic formula derived from the Shannon theorem and the capacity using the sum of the sub–channel capacities. We have proved that these two capacities are equal. Moreover, we have calculated the

radiation patterns for the elements in the RX and TX arrays. The pattern confirmed the orthogonal decomposition of the SVD as the patterns of the elements within the array were complementary. Finally, we have confirmed these results by the measurement in the anechoic chamber.

The fifth chapter is dedicated to the measurement of the channel capacity in a real scenario. The measurement was based on the impulse response measurement using the Vector Network Analyzer (VNA). Three scenarios in total were presented in the section. The static scenario in the corridor was designed as very similar to the measurement in the anechoic chamber, while both LOS and NLOS cases were measured. The capacity results were presented as for the SNR as a parameter. The achieved capacity for the LOS was estimated as slightly higher than the NLOS capacity as it is expected. However, the difference was found not so significant as the MIMO utilized in the NLOS. The radiation patterns were presented as well, proving the orthogonal decomposition into independent channels once again.

The dynamic scenario was illustrating the dependence of the channel capacity on the movement between the antennas. The antennas were placed in the crowded corridor, and 501 snapshots within four seconds were taken. Therefore, the mean and standard deviation of the capacity from the histogram were calculated; the mean value equals 36.3 bit/s/Hz, and standard deviation equals 2.37 bit/s/Hz. The capacity is estimated using the channel matrix obtained as an expected value of the channel responses between the antennas.

The quasi–dynamic scenario presented the moving antenna as emulating of the pedestrian movement inside the corridor. Twenty measurements within 130 centimeters were obtained, and histogram of the measurements was presented and used for the calculation of the mean value, and standard deviation; the mean value equals 38.82 bit/s/Hz and standard deviation equals 1.21 bit/s/Hz. The capacity was estimated the same way as in the previous scenario using the expected value of channel responses. The expected value of the capacity in the dynamic scenario with no permanent obstruction of the LOS is higher that the capacity in the quasi–dynamic scenario where the obstruction is permanently placed between the antenna arrays.

The eigenvalue decomposition for coding in the wireless systems was studied, simulated and applied in the real scenario measurements of the MIMO channel capacity. The main benefit of the eigenvalue decomposition is in estimating the orthogonal sub–channels of the wireless channel and sending the data through these sub–channels with minimum error rates. The work utilizes SVD as the tool of the decomposition in real scenario measurements to estimate the channel capacity. The comparison of the estimated capacity between the LOS and NLOS static scenarios were presented; the capacity of the MIMO

channel for LOS is higher than the capacity in the NLOS case. Two other dynamic scenarios were measured and the capacity for the cases was estimated. As the standard deviation in the second scenario is lower than in the third scenario, we find the capacity of the dynamic scenario with the pedestrian movement between the antennas more stable than the quasi–dynamic scenario where one antenna was moving towards the other antenna. However, the expected values of the capacities estimated from the mean values of the impulse responses are very similar.

Bibliography

[1] H. Jafarkhani, Space-time coding: theory and practice. Cambridge university press, 2005.

[2] B. Kumbhani and R. S. Kshetrimayum, MIMO wireless communications over generalized fading channels. CRC Press, 2017.

[3] A. F. Molisch, Wireless communications. John Wiley & Sons, 2012, vol. 34.

[4] D. Tse and P. Viswanath, Fundamentals of wireless communication. Cambridge university press, 2005.

[5] J. Sykora, Space-time communications (lecture), 2018.

[6] S. Ranvier, J. Kivinen, and P. Vainikainen, "Development of a 60 ghz mimo radio channel measurement system", in 2005 IEEE Instrumentationand Measurement Technology Conference Proceedings, vol. 3, 2005, pp. 1878–1882. DOI: 10.1109/IMTC.2005.1604498.

[7] J. Kivinen, M. Karkkainen, P. Kangaslahti, and X. Zhao, "Wideband radio channel sounder extension to 60 GHz frequency range", in 31st European Microwave Conference, 2001, IEEE, 2001, pp. 1–4. DOI: 10.1109/euma.2001.339105. [Online]. Available: https://doi.org/10.1109/euma.2001.339105.

[8] K. Sulonen, P. Suvikunnas, L. Vuokko, J. Kivinen, and P. Vainikainen, "Comparison of mimo antenna configurations in picocell and microcell environments", IEEE Journal on Selected Areas in Communications, vol. 21, no. 5, pp. 703–712, 2003, ISSN: 0733-8716. DOI: 10.1109/JSAC.2003.810297.

[9] A. A. Kalachikov and I. V. Bashkatov, "Experimental channel parameters and capacity measurement of wireless mimo channel at 2.4 ghz", in 2014 12th International Conference on Actual Problems of Electronics Instrument Engineering (APEIE), 2014, pp. 346–348. DOI: 10.1109/APEIE.2014.7040913.

[10] P. L. Kafle, A. Intarapanich, A. B. Sesay, J. Mcrory, and R. J. Davies, "Spatial correlation and capacity measurements for wideband mimo channels in indoor office environment", IEEE Transactions on Wireless Communications, vol. 7, no. 5, pp. 1560–1571, 2008, ISSN: 1536-1276. DOI: 10.1109/TWC.2008.060170.

[11] T. S. Rappaport et al., Wireless communications: principles and practice. prentice hall PTR New Jersey, 1996, vol. 2.

[12] D. Chizhik, G. J. Foschini, M. J. Gans, and R. A. Valenzuela, "Keyholes, correlations, and capacities of multielement transmit and receive antennas", IEEE Transactions on Wireless Communications, vol. 1, no. 2, pp. 361–368, 2002, ISSN: 1536-1276. DOI: 10.1109/7693.994830.

[13] A. Zangwill, Modern electrodynamics. Cambridge University Press, 2013.

[14] S. Saunders and A Aragón-Zavala, "Antennas and propagation for wireless communication systems, 2007", International Journal of Aerospace Engineering Hindawi Publishing Corporation http://www. hindawi. com, vol. 2014,

Extra

Content of the .zip file

The .zip file is enclosed with the work, which contains:

- Root directory: contains the thesis in format of .pdf
- Directory MATLAB: contains scripts for the simulation, scripts for processing the measured data and altered measured data
- Directory DATA: contains raw data from the VNA